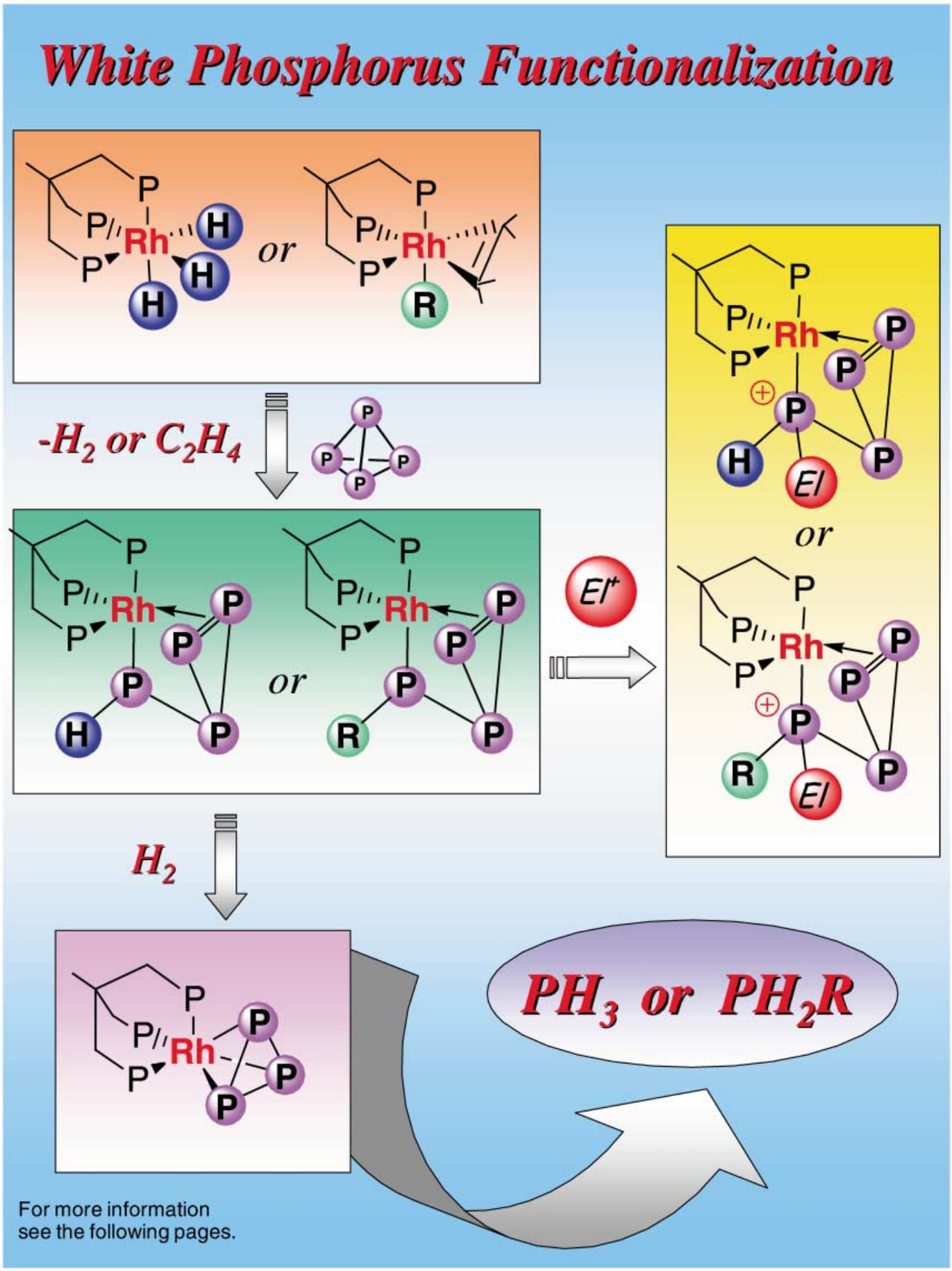

 DOI: 10.1002/chem.200305091

Activation and Functionalization of White Phosphorus at Rhodium: Experimental and Computational Analysis of the [(triphos)Rh(η^1:η^2-P_4RR')]Y Complexes (triphos = $MeC(CH_2PPh_2)_3$; R = H, Alkyl, Aryl; R′ = 2 Electrons, H, Me)

Pierluigi Barbaro,[a] Andrea Ienco,[a] Carlo Mealli,[a] Maurizio Peruzzini,*[a] Otto J. Scherer,[b] Guido Schmitt,[b] Francesco Vizza,*[a] and Gotthelf Wolmershäuser[b]

Omnia mutantur, nihil interit (Ovidius, *Metamorphosis*, XV, 165).
We dedicate this paper to the memory of José Antonio Ramirez (1957–2000), Professor of Chemistry at the University of Valencia (Spain). His enthusiasm and his excellence in NMR computing was crucial in pursuing and developing this chemistry.

Abstract: Thermal reaction of white phosphorus with [(triphos)RhH_3] (**1**) in THF affords [(triphos)Rh(η^1:η^2-P_4H)] (**2**), triphos = $MeC(CH_2PPh_2)_3$. Similar complexes [(triphos)Rh(η^1:η^2-P_4R)] (R = Me (**7**), Et (**8**), Ph (**9**)) also form at lower temperature by the reaction of P_4 and [(triphos)Rh(R)(η^2-C_2H_4)] with elimination of ethene. In contrast, a double-insertion process follows the reaction of [(triphos)Rh(H)(η^2-C_2H_4)] and P_4 to generate tetraphosphido ethyl complex **8**. Compounds **2**, **7**, **8** and **9** are thermally unstable and eventually decompose into the cyclotriphosphorus complex [(triphos)Rh(η^3-P_3)] (**3**) plus other unidentified phosphorus-containing species. Otherwise, PH_3 or PH_2R is generated in the presence of H_2. The formation of PH_3 and **3** is quantitative starting from the precursor **2**. The electrophilic attack of MeOTf or HBF_4 on the P_4R ligand in the complexes **2**, **7**–**9** is regioselective, and yields a cationic product of formula [(triphos)Rh(η^1:η^2-P_4RR')]$^+$. The direct attack on the substituted *p*-R phosphorus atom is demonstrated by crossing experiments. Complexes of the latter type have been isolated in the solid state for the combinations R = H and R′ = Me (**11**) or R = Ph and R′ = Me (**12**). The latter species, [(triphos)Rh(η^1:η^2-P_4PhMe')]OTf·$2CH_2Cl_2$ (OTf = triflate), has been characterised by X-ray methods. The geometry at the metal is better described as a trigonal bipyramidal than pseudo-octahedral. In fact, the P_4RR' unit acts as a bidentate ligand with its exocyclic PR_2 donor group and the endocyclic, dihapto-coordinated P=P linkage. The latter group lies in the equatorial plane, in a similar way to a classic olefin ligand that is coordinated to a butterfly-shaped L_4M fragment ($M = d^8$). DFT calculations on a model of **2** and all possible protonated isomers confirm that double substitution at the exocyclic P-donor positions of the open P_4 unit is energetically favoured. A multinuclear and multidimensional NMR analysis confirms that this structure is maintained in solution for both the parent and the protonated compounds.

Keywords: density functional calculations · NMR spectroscopy · phosphorus · polyphosphines · rhodium

Introduction

The selective activation of phosphorus–phosphorus bonds and their functionalisation by transition metal complexes have recently attracted much interest for their potential applications in the industrial synthesis of organophosphorus compounds.[1] The catalytic functionalisation of white phosphorus by transition metals remains an important challenge, particularly in view of the environmental drawbacks of certain industrial processes. In fact, the current manufacturing of organophosphorus compounds is incompatible with "green chemistry" as it is based on the chlorination of white phosphorus to PCl_3 or $POCl_3$. The process is then followed by alkylation with Grignard reagents to form the P–C linkages.[2]

The P–P bonds of P_4 are reactive enough, as they are cleaved under relatively mild homogeneous conditions. For instance, the oxidative addition of a P–P bond can be done stoichiometrically by using a variety of transition metal moieties. When the reaction conditions are not severe, complexes with a formally inactivated η^2-P_4 ligand, such as the Krossing silver salt $Ag(\eta^2\text{-}P_4)_2^+$, may be synthesised.[3] More frequently, however, complexes that contain the

[a] Dr. M. Peruzzini, Dr. F. Vizza, Dr. P. Barbaro, Dr. A. Ienco, Dr. C. Mealli
Istituto di Chimica dei Composti Organometallici, ICCOM-CNR
Via Madonna del Piano, Polo Scientifico di Sesto Fiorentino
50018 Sesto Fiorentino (Italy)
Fax: (+39) 055-25252-203
E-mail: mperuzzini@iccom.cnr.it, francesco.vizza@iccom.cnr.it

[b] Prof. Dr. O. J. Scherer, Dr. G. Schmitt, Dr. G. Wolmershäuser
University of Kaiserslautern, Department of Chemistry
Erwin Schrödinger Strasse, 67663 Kaiserslautern (Germany)

DOI: 10.1002/chem.200305091

activated P_4^{2-} tetraphosphabutadienyl species, are stabilised. The latter dianion may either act as a η^2-chelate, such as in the Ginsberg and Lindsell derivative $[(PPh_3)_2ClRh(\eta^2\text{-}P_4)]$,[4, 5] or as a η^1,η^1-bridging unit that was first discovered by Scherer in the binuclear complex $[\{(1,3\text{-}Bu^t\text{-}Cp)Fe(CO)_2\}_2(\mu,\eta^{1:1}\text{-}P_4)]$.[6] In contrast, when more drastic conditions are adopted, such as in the typical thermal or photochemical reactions of P_4 with transition-metal systems, the initially formed P–P adducts, may easily undergo disruptive and/or reconstructive processes. As a result, a spectacular variety of transition metal complexes may be formed that contain a P_x ligand with x ranging from 1 to 12.[7]

In spite of the many fundamental studies that concern the activation of the P_4 molecule, the metal-mediated functionalisation of this phosphorus allotrope has received much less attention, and the construction of both P–C and P–H bonds directly from white phosphorus remains a significant challenge.[8, 9]

As a part of our on-going interest in the coordination chemistry of white phosphorus,[10, 11] we now illustrate a system based on the (triphos)Rh fragment [triphos = tripodal phosphine $MeC(CH_2PPh_2)_3$] that supports a P–H- or a P–C-functionalised tetraphosphorus ligand. A multidisciplinary approach has been followed for the characterisation of the various complexes and includes NMR spectroscopy, X-ray crystallography and DFT calculations. We complete the report on this chemistry,[12] which is based on the transfer of a Rh–H or Rh–C bond to the metal-activated P_4 molecule, by providing information about possible reactivity patterns. These patterns seem to be particularly significant for the design of environmentally acceptable "chlorine-free" approaches to the catalytic synthesis of organophosphorus compounds.[1, 13]

Experimental Section

General data: All reactions and manipulations were routinely performed under a dry nitrogen or argon atmosphere by using standard Schlenk techniques. Tetrahydrofuran (THF) was freshly distilled over $LiAlH_4$, acetone and benzene were distilled over P_2O_5, dichloromethane and methanol were purified by distillation over CaH_2 before use, *n*-hexane was stored over molecular sieves and purged with nitrogen prior to use. The complexes $[(triphos)RhH_3]$,[14] and $[(triphos)Rh(R)(C_2H_4)]$ (R = H, Me, Et, Ph)[15] were prepared as previously reported. The perdeuterated hydride, $[(triphos)RhD_3]$, was prepared as described for the protiated analogue,[16] but with deuterated solvents and reagents. White phosphorus was mechanically cleaned from oxide layers, washed with THF and dried in a stream of nitrogen. All the other reagents and chemicals were reagent grade and, unless otherwise stated, were used as received from commercial suppliers. The solid complexes were collected on sintered-glass frits and washed with *n*-pentane before being dried in a stream of nitrogen, unless otherwise stated. IR spectra were obtained in Nujol mull or in dichloromethane solution by using a 0.2 mm NaCl cuvette on a Perkin–Elmer 1600 series FTIR spectrophotometer (4000–200 cm^{-1}). Deuterated solvents for NMR measurements (Aldrich and Merck) were dried over molecular sieves (4 Å). MS spectral data of $[(triphos)Rh\{\eta^1\text{:}\eta^2\text{-}P_4Ph(Me)\}]OTf$ (**12**) were recorded on a Finnigan MAT90 spectrometer (EI-pos, 70 eV, 0.3 mA). Elemental analyses (C, H, N) were performed by using a Carlo Erba model 1106 (ICCOM CNR) and a Perkin–Elmer C,H,N-Analyser (University of Kaiserslautern) elemental analyser.

NMR experiments: $^{31}P\{^1H\}$, ^1H and $^{13}C\{^1H\}$ NMR spectra (see Tables 3–5, below) were recorded on a Bruker ACP200 spectrometer operating at 81.01, 200.13 and 50.32 MHz, respectively, or on a Bruker Avance DRX-500 spectrometer equipped with a variable-temperature control unit accurate to $\pm 0.1\,^\circ C$ and operating at 202.47, 500.13 and 125.76 MHz, respectively. $^{31}P\{^1H\}$ chemical shifts are relative to external 85% H_3PO_4 with downfield values reported as positive. ^1H and $^{13}C\{^1H\}$ chemical shifts are relative to tetramethylsilane as external reference and were calibrated against the residual solvent resonance (^1H) or the deuterated solvent multiplet (^{13}C). The assignments of the signals resulted from 1D spectra, 2D ^1H-DQF COSY, $^{31}P\{^1H\}$ COSY, ^1H NOESY and proton-detected 2D $^1H-^{13}C$ and $^1H-^{31}P$ correlations. 2D NMR spectra were recorded on a Bruker Avance DRX-500 spectrometer on degassed nonspinning samples with pulse sequences suitable for phase-sensitive representations by using time-proportional phase incrementation. J_{HH} and J_{HP} coupling constants were obtained from 1D $^1H\{^1H\}$ homonuclear and selective $^1H\{^{31}P\}$ heteronuclear decoupling experiments, J_{CP} coupling constants were obtained from 1D $^{13}C\{^1H\}$ and $^{13}C\{^1H\}\{^{31}P\}_{sel}$ spectra, J_{PP} and J_{PRh} coupling constants were obtained with the aid of computer simulation by using the *gNMR* program.[17] Standard pulse sequences were used for the ^1H-DQF COSY[18] and ^1H NOESY[19] experiments: 1024 increments of size 2 K (with 8 scans each) covering the full range in both dimensions (ca. 5000 Hz) were acquired with a relaxation delay of 2 s and a mixing time of 1.0 or 0.8 s. The $^{31}P\{^1H\}$ COSY measurements were recorded with ^1H decoupling during acquisition: 1024 increments of size 2 K (with 16 scans each) covering the full range in both dimensions (ca. 60000 Hz) were collected with a relaxation delay of 0.8 s The $^1H-^{13}C$ correlations were recorded by using both Heteronuclear Multiple Quantum Coherence (HMQC)[20] and Heteronuclear Multiple Bond Coherence (HMBC)[21] sequences with no decoupling during acquisition, 1024 increments of size 2 K (with 16 scans each) were collected covering the full range in both dimensions (ca. 5000 Hz in *F*2 and 22000 Hz in *F*1) with a relaxation delay of 2.0 s. A low-pass *J* filter was used to suppress one-bond correlations in the HMBC experiments. The $^1H-^{31}P$ correlations were recorded by using the standard HMQC sequence[22] with ^1H decoupling during acquisition, 1024 increments of size 2 K (with 8 scans each) were collected covering the full range in both dimensions with a relaxation delay of 2.0 s. Experiments were optimised for the detection of J_{HP} couplings of 5 and 15 Hz.

The high-pressure NMR (HPNMR) experiments were performed in 10 mm sapphire tubes (Saphikon Inc., NH, USA) assembled with an in-house-built Ti-alloy pressure head.[23] The HPNMR spectra were recorded by using a standard 10 mm probe tuned to ^{31}P and ^1H on a Bruker AC200 spectrometer at ICCOM CNR.

CAUTION: *All manipulations involving high pressures are potentially hazardous. Safety precautions must be taken at all stages of NMR studies involving high-pressure NMR tubes.*

Reaction of $[(triphos)RhH_3]$ with white phosphorus

Open-system reaction: Solid white phosphorus (0.25 g, 2.02 mmol) was added to a suspension of $[(triphos)RhH_3]$ (**1**) (0.73 g, 1.00 mmol) in THF (50 mL). The mixture was stirred at room temperature under nitrogen for 20 min and then heated under reflux for 2 h. After the solvent had been evaporated under vacuum, the residue was washed with ethanol (3×5 mL) and pentane (3×5 mL). $[(triphos)Rh(\eta^1\text{:}\eta^2\text{-}P_4H)]$ (**2**) was collected by filtration as a yellowish orange microcrystalline material, which was washed with pentane (3×5 mL) before being dried under a stream of nitrogen. Yield: 0.62 g (73%); IR (Nujol): $\tilde{\nu}=2213$ (w) cm^{-1} (PH); elemental analysis calcd (%) for $C_{41}H_{40}P_7Rh$: C 57.77, H 4.73, P 25.43; found C 57.56, H 4.70, P 25.28.

Replacing **1** with $[D_3]$**1** in the above procedure gave [D]**2** in similar yield.

Closed-system reaction: A 100 mL Parr autoclave was charged with white phosphorous (0.12 g, 1.01 mmol), $[(triphos)RhH_3]$ (0.37 g, 0.5 mmol) and THF (50 mL). The mixture was stirred at room temperature for 30 min and then heated to 70 °C for 2 h before being cooled to ambient temperature. The volatiles were slowly released under nitrogen and absorbed into a 5 mm NMR tube containing $[D_8]$THF (1.0 mL) cooled to −78 °C. $^{31}P\{^1H\}$ NMR analysis showed the formation of PH_3 [^{31}P $\delta=-244.77$, q, $J(PH)=186.9$ Hz]. The contents of the reactor were transferred to a Schlenk flask and then evaporated under vacuum. The yellowish orange residue was washed with pentane (3×5 mL) and recrystallised from a dichloromethane/ethanol mixture (2:1, *v*/*v*) to yield a yellow microcrystalline sample of $[(triphos)Rh(\eta^3\text{-}P_3)]$ (**3**). Yield 76%. The nature of **3** was ascertained by

comparison of its physico-chemical properties with those of an authentic specimen.[24]

In situ HPNMR hydrogenation of [(triphos)Rh(η¹:η²-P₄H)]: A 10 mm sapphire HPNMR tube was charged with **2** (20 mg, 2.34×10^{-2} mmol), degassed [D₈]THF (1.8 mL) and then pressurised with hydrogen gas (2 atm) at 0 °C. The experiment was started by heating the probe to 70 °C for 1 h. ^{31}P NMR analysis showed the complete transformation of **2** into **3** and PH_3. The resulting solution was poured into a Schlenk tube, and the solvent was removed under vacuum to leave **3** as a yellowish powdered material, which was washed with ethanol (2×2 mL) and *n*-pentane (2×1 mL). Yield 93 %.

Reaction of [(triphos)Rh(R)(η²-C₂H₄)] (R = Me (4), Et (5), Ph (6)) with white phosphorus. Synthesis of [(triphos)Rh(η¹:η²-P₄R)] complexes: A solution of the appropriate rhodium complex [(triphos)Rh(R)(η²-C_2H_4)] (R = Me (**4**), Et (**5**), Ph (**6**)) (1.0 mmol) in THF (30 mL) was stirred at room temperature under nitrogen in the presence of a twofold excess of white phosphorus (250 mg, 2.02 mmol) predissolved in THF (10 mL). Immediately, the light yellow solution turned deep orange. Stirring was continued for another 10 min, and then the solvent and the volatile components were evaporated to dryness under vacuum leaving a red-orange residue, which was washed with *n*-pentane (3×5 mL) before being dried at room temperature under a stream of nitrogen. Recrystallisation from THF/*n*-hexane (1:3 *v*/*v*) was performed to obtain analytically pure microcrystals of [(triphos)Rh(η¹:η²-P_4R)] (R = Me (**7**), Et (**8**), Ph (**9**)) in moderate yield (ca. 60 – 70 %). Compounds **7** – **9** are stable at room temperature in the solid state under nitrogen atmosphere but slowly decompose in solution above 10 °C. The decomposition is more rapid at temperatures higher than 45 °C.

[(triphos)Rh(η¹:η²-P₄Me)] (7): Yield 67 %; elemental analysis calcd (%) for $C_{42}H_{42}P_7Rh$: C 58.45, H 4.96; found C 58.22, H 4.89.

[(triphos)Rh(η¹:η²-P₄Et)] (8): Yield 66 %; elemental analysis calcd (%) for $C_{43}H_{44}P_7Rh$: C 58.78, H 5.19; found C 58.65, H 5.04.

[(triphos)Rh(η¹:η²-P₄Ph)] (9): Yield 71 %; elemental analysis calcd (%) for $C_{47}H_{44}P_7Rh$: C 61.01, H 4.89; found C 60.77, H 4.78.

Reaction of [(triphos)Rh(H)(η²-C₂H₄)] (10) with white phosphorus: A solution of [(triphos)Rh(H)(η²-C_2H_4)] (700 mg, 0.92 mmol) in THF (30 mL) was treated with an excess of white phosphorus (250 mg, 2.02 mmol) as described previously. Standard work-up gave the product **8** as red microcrystals. Yield 78 %.

General procedure for the preparation of [(triphos)Rh(η¹:η²-P₄RR′)]OTf: One equivalent of the appropriate electrophile (neat HOTf or MeOTf) was syringed under argon into a stirred solution of [(triphos)Rh(η¹:η²-P_4R)] (R = H (**2**), Me (**7**), Ph (**9**)) in THF (25 mL) protected from light by wrapping the reaction vessel with aluminium foil. The solution was stirred for one hour at room temperature in the dark, during which time the formation of a bright yellow crystalline compound was observed. The solvent was concentrated to approximately half volume under vacuum, and *n*-hexane (10 mL) was added to complete the precipitation. After an additional 30 min stirring, the yellowish orange microcrystalline material that separated out was collected on a sintered-glass frit and washed with *n*-pentane (50 mL). The product yield ranged from 64 to 77 %. Compounds **11** and **12** were stored in Schlenk flasks under argon at −20 °C without apparent decomposition over several weeks.

[(triphos)Rh(η¹:η²-P₄HMe)]OTf (11)

Method A: [(triphos)Rh(η¹:η²-P_4H)] (**2**) (256 mg, 0.30 mmol)/MeOTf (34 μL, 0.31 mmol); yield 69 %.

Method B: [(triphos)Rh(η¹:η²-P_4Me)] (**7**) (250 mg, 0.29 mmol)/HOTf (26 μL, 0.29 mmol); yield 64 %; elemental analysis calcd (%) for $C_{43}H_{43}F_3O_3P_7RhS$: C 50.79, H 4.27; found C 51.10, H 4.46.

[(triphos)Rh(η¹:η²-P₄PhMe)]OTf (12): [(triphos)Rh(η¹:η²-P_4Ph)] (**9**) (280 mg, 0.30 mmol)/MeOTf (34 μL, 0.31 mmol), yield 77 %; elemental analysis calcd (%) for $C_{49}H_{47}F_3O_3P_7RhS$: C 53.86, H 4.34; found C 54.08, H 4.50. Crystals of **12** suitable for X-ray analysis were grown at room temperature under nitrogen from a dilute dichloromethane solution.

The iodide salt [(triphos)Rh(η:η²-P_4PhMe)]I (**12**-I) was prepared with the same procedure by using CH_3I (15 μL, 0.31 mmol) in place of MeOTf . Identical work-up gave **12**-I in ca. 74 % yield. Elemental analysis calcd (%) for $C_{48}H_{47}IP_7Rh$: C 53.85, H 4.43; found C 53.96, H 4.59.

Crystal data and structure refinement of [(triphos)Rh(η¹:η²-P₄PhMe)]-OTf·2CH₂Cl₂ (12·2CH₂Cl₂): Crystal data for complex **12**·$2CH_2Cl_2$ are reported in Table 1 while selected bond lengths and angles are reported in Table 2.

Table 1. Crystal data for [(triphos)Rh(η¹:η²-P_4PhMe)]OTf·$2CH_2Cl_2$ (**12**·$2CH_2Cl_2$)

empirical formula	$C_{51}H_{51}Cl_4F_3O_3P_7RhS$
crystal size [mm]	$0.40 \times 0.32 \times 0.16$
M_r	1262.48
T [K]	293(2)
λ [Å]	0.71073
crystal system	triclinic
space group	$P\bar{1}$
a [Å]	11.6837(18)
b [Å]	14.967(3)
c [Å]	17.598(3)
α [°]	112.460(18)
β [°]	91.420(18)
γ [°]	93.75(2)°
V [Å^3]	2833.8(8)
Z	2
ρ_{calcd} [Mg m^{-3}]	1.480
μ [mm^{-1}]	0.775
$F(000)$	1284
θ range	2.73 to 25.68°
limiting indices	$-14 \le h \le 14$, $-18 \le k \le 18$, $-21 \le l \le 21$
reflections collected/unique	28620/10117
R(int)	0.1157
completeness to θ	25.68° / 93.8 %
data/restraints/parameters	10117/72/597
goodness-of-fit on F^2	0.975
final R indices [$I > 2\sigma(I)$]	
$R1$	0.0657
$wR2$	0.1785
R indices (all data)	
$R1$	0.0912
$wR2$	0.1915
weighting scheme $w = 1/[\sigma^2(F_o^2) + (0.1200P)^2]$ $P = (F_o^2 + 2F_c^2)/3$	
largest difference peak and hole [e Å^{-3}]	1.415 and −1.095

Table 2. Selected bond lengths [Å] and angles [°] for [(triphos)Rh(η¹:η²-P_4PhMe′)]OTf·$2CH_2Cl_2$ (**12**·$2CH_2Cl_2$).

Rh1−P6	2.351(2)	Rh1−P5	2.365(2)
Rh1−P4	2.369(2)	Rh1−P7	2.373(2)
Rh1−P3	2.441(2)	Rh1−P2	2.449(2)
P1−P4	2.165(2)	P1−P2	2.232(3)
P1−P3	2.242(3)	P2−P3	2.123(3)
P6-Rh1-P5	88.83(6)	P6-Rh1-P4	97.56(6)
P5-Rh1-P4	165.14(5)	P6-Rh1-P7	90.66(6)
P5-Rh1-P7	86.27(6)	P4-Rh1-P7	106.96(6)
P6-Rh1-P3	108.45(7)	P5-Rh1-P3	87.93(6)
P4-Rh1-P3	77.34(6)	P7-Rh1-P3	159.91(6)
P6-Rh1-P2	159.90(7)	P5-Rh1-P2	90.18(6)
P4-Rh1-P2	79.20(6)	P7-Rh1-P2	109.31(7)
P3-Rh1-P2	51.46(7)	P4-P1-P2	88.63(9)
P4-P1-P3	85.99(9)	P2-P1-P3	56.65(9)
P3-P2-P1	61.92(9)	P3-P2-Rh1	64.08(7)
P1-P2-Rh1	88.82(8)	P2-P3-P1	61.43(9)
P2-P3-Rh1	64.47(7)	P1-P3-Rh1	88.78(7)

All the crystals from different batches were multiply twinned. A suitable crystal was mounted in a Lindemann tube on a Stoe IPDS diffractometer. Data were collected at ambient temperature with monochromatised $Mo_{K\alpha}$ radiation by using ϕ oscillation scans. Intensities were corrected by

analytical absorption correction. Accurate cell parameters were obtained from 7998 reflections. The structure was solved by SHELXS-97[25] by direct methods. The remaining non-hydrogen atoms were located by successive Fourier difference maps. The structure was refined with the SHELXL-97[25] program package. All non-hydrogen atoms, except those of the disordered anion, were refined anisotropically. Hydrogen atoms, at calculated positions, were included in the final stages of refinement with constrained isotropic thermal parameters. Software used for molecular graphics: SHELXTL (XP).[26]

CCDC-202463 contains the supplementary crystallographic data for this paper. These data can be obtained free of charge via www.ccdc.cam.ac.uk/conts/retrieving.html (or from the Cambridge Crystallographic Data Centre, 12 Union Road, Cambridge CB2 1EZ, UK; fax: (+44) 1223-336033; or deposit@ccdc.cam.uk).

Computational details: Structural optimisations were carried out by using hybrid density-functional theory (DFT) with Becke's three-parameter hybrid exchange-correlation functional[27] containing the nonlocal gradient correction of Lee, Yang and Parr (B3LYP)[28] within the Gaussian 98 program.[29] The natures of the optimised structures were confirmed by calculations of the vibrational frequencies. A collection of Cartesian coordinates and total energies for all of the optimised molecules are available from the authors upon request. The basis set for the Rh atom utilised the effective core potentials of Hay and Wadt[30] with the associated double-ζ valence basis functions. The 6-31G(d, p) basis set was used for the remaining atomic species.[31]

The ligand triphos was best modelled by replacing all of the phenyl substituents with H atoms (Htriphos). This simplifies the computational task, while maintaining the typical geometric constraints at the metal. In particular, the three P-Rh-P angles are forced to be almost 90°.

It is worth mentioning that preliminary calculations with three independent PH_3 ligands for modelling the triphos ligand gave similar results in term of energetic trends (with respect to the calculations with Htriphos, the important ΔEs are never greater than 2 kcal mol^{-1}). However, these simplified models are without the 90° constrains at the P-Rh-P angles (the equatorial one is as large as 106°), so that the models were considered unsatisfactory for mimicking the actual geometry of the (triphos)Rh fragment.

Extended Hückel calculations[32] were carried out in order to gain a simple overview of the major interactions between fragments and of the MO evolution for structural rearrangements (interaction and Walsh diagrams). The consistency of some basic results, with respect to those of the DFT method, is also shown by the drawings of the frontier MOs generated by the package CACAO,[33] which are essentially similar to those generated by DFT. The EHT input files was generated using the DFT optimised models.

Results and Discussion

Reactivity of the [(triphos)Rh(R)] synthon with white phosphorus. Synthesis of the [(triphos)Rh(η^1:η^2-P_4R)] complexes 2 (R = H), 7 (Me), 8 (Et) and 9 (Ph)

Reaction of white phosphorus with [(triphos)RhH$_3$]: The thermal reaction between [(triphos)RhH$_3$] (**1**) and white phosphorus under nitrogen in THF at refluxing temperature led to an orange solution from which yellow-orange microcrystals of [(triphos)Rh(η^1:η^2-P_4H)] (**2**) were obtained in good yield after solvent evaporation under reduced pressure (Scheme 1).

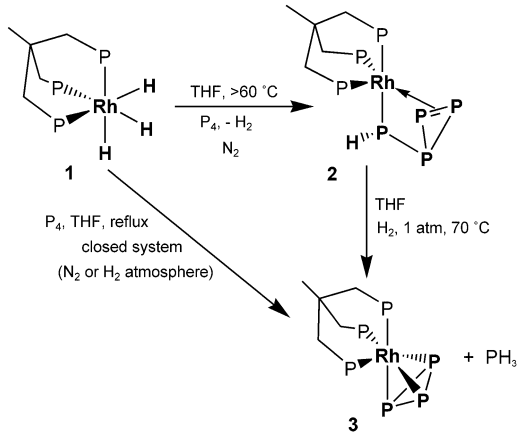

Scheme 1.

The presence of the unprecedented η^1:η^2-P_4H ligand in **2** was established by IR and multinuclear, multidimensional NMR spectroscopies. However, the detailed structural features, which, due to the lack of suitable crystals, could not be determined by X-ray diffraction methods, have been assessed by DFT calculations (vide infra). On the basis of the latter, we anticipate that the geometry of **2** may be best described as a trigonal bipyramid in which an η^1:η^2-P_4H monoanionic ligand acts as a four-electron donor towards the rhodium(I) metal. The situation is sketched in Scheme 2.

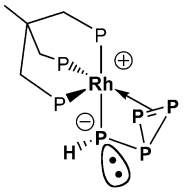

Scheme 2.

In the IR spectrum, a weak band at 2213 cm^{-1} was ascribed to the P–H stretching vibration. In keeping with this assignment, the absorption was absent in the IR spectrum of [(triphos)-Rh(η^1:η^2-P_4D)] ([D]**2**), which was obtained by replacing the reactant **1** with [D_3]**1**.

In agreement with the complete incorporation of four P_4 phosphorus atoms into the metal complex, an ABCDEFGX spin system was observed in the $^{31}P\{^1H\}$ NMR spectrum of **2** ([D_8]THF). Analysis of the $^{31}P\{^1H\}$ COSY spectrum allowed us to determine the network of P–P connections and to carry out complete simulation of the seven different multiplets appearing in the $^{31}P\{^1H\}$ spectrum. ^{31}P NMR DEPT experiments, (DEPT90 and DEPT135) together with ^{1}H,^{31}P NMR measurements, confirmed the presence of the monohydrotetraphosphido unit (vide infra NMR section).

By monitoring in situ the reaction between **1** and white phosphorus (1:2 in [D_8]THF), $^{31}P\{^1H\}$ NMR spectroscopy showed that complex **2** begins to form at about 40 °C following the thermal extrusion of H_2 ($\eta_{H_2} = 4.75$ ppm in the ^{1}H NMR spectrum) and the rhodium-to-phosphorus migration of the third hydride ligand of **1**. At higher temperature (> 70 °C), complex **2** transforms quantitatively into the known *cyclo*-triphosphorus species [(triphos)Rh(η^3-P_3)] (**3**).[24] Noticeably, the appearance of **3** in the spectrum was accompanied by the growth of a singlet at −244.77 ppm that is attributable to the formation of one equivalent of PH_3. Further evidence for the assignment is the splitting of this resonance into a binomial quartet once the broadband ^{1}H decoupler is switched off [^1J(P,H) ≈ 187 Hz]. To support the feasibility of a process that encompasses the hydrogenation of the intermediate η^1:η^2-P_4H complex **2**, a separate NMR experiment was carried out. Thus it was shown that **2** readily reacts with hydrogen ($p_{H_2} = 1$ atm) at about 70 °C in [D_8]THF solution to selectively form **3** and phosphine. By replacing **1** with [D_3]**1**, the in situ NMR

experiment showed that the perdeuterated PD_3 phosphine is formed together with complex **3**. This confirms that all three hydride hydrogen atoms in **1** were selectively transferred during the reaction to the same phosphorus atom of the P_4 tetrahedron.

Reaction of white phosphorus with [(triphos)Rh(R)(C_2H_4)]: In order to explore the reactivity of white phosphorus with related organometallic species that contain ligands other than hydrides, we investigated the reactivity of the complexes [(triphos)Rh(R)(C_2H_4)] (R = Me (**4**), Et (**5**), Ph (**6**)). In this manner, the known lability of the ethene ligand can be exploited,[15] hence the coordinatively unsaturated residue [(triphos)Rh(R)] can mimic the [(triphos)RhH] fragment with respect to reactivity towards P_4. In keeping with our expectations, when a solution of **4**, **5** or **6** in THF was treated with a twofold molar amount of P_4 at room temperature under nitrogen, the complexes [(triphos)Rh(η^1:η^2-P_4R)] (R = Me (**7**), Et (**8**), Ph (**9**)) were obtained in excellent yield (Scheme 3). The reactions were accompanied by a colour

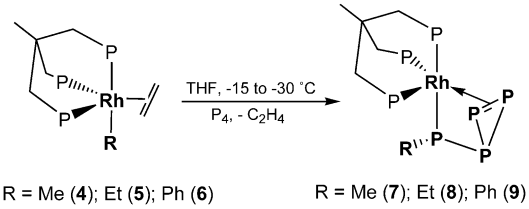

Scheme 3.

change from pale yellow to deep orange. The $^{31}P\{^1H\}$ NMR spectra of all compounds **7**–**9** showed eight well-separated multiplets forming a rather complicated ABCDEFGX spin system that closely resembled that mentioned for **2**. This piece of information clearly suggests that, analogously to **2**, all of the four phosphorus atoms originating from the P_4 unit have been incorporated into the final products and that the resulting compounds lack any high-symmetry elements, that is, all of the phosphine groups of triphos are chemically nonequivalent. A perusal of the NMR data (vide infra NMR section) definitely supported the proposed structures of **7**–**9** and clearly indicated that once ethene is released from rhodium, the final product forms through the selective migration of the R group from the metal atom to one of the four phosphorus atoms of the activated P_4 fragment.

On monitoring the reaction between the complexes **4**–**6** and white phosphorus in [D_8]THF (in situ NMR experiment), no intermediate was detected in the process leading to the formation of η^1:η^2-P_4R species **7**–**9**. Thus, the straightforward formation of the reaction products took place as soon as the [D_8]THF solutions of the rhodium complex and white phosphorus were mixed at low temperature (−30 °C for **4** and **5**, −15 °C for **6**). The signal due to free ethene in solution was observed in the proton spectrum as a slightly broadened singlet at about 5.50 ppm.

A reaction analogous to that depicted in Scheme 3 was expected when using [(triphos)Rh(H)(C_2H_4)] (**10**) as a reactant. However, as shown in Scheme 4, the product of

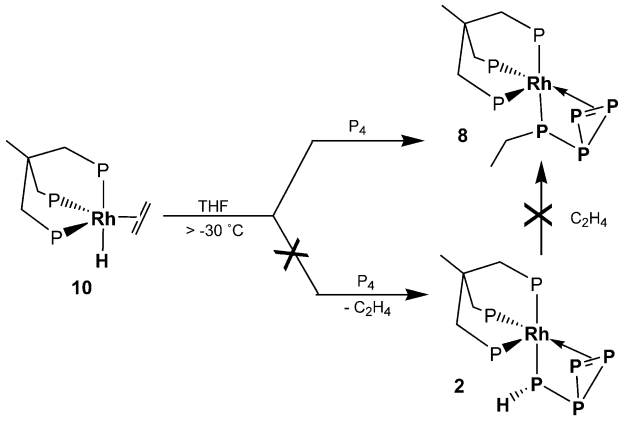

Scheme 4.

the reaction with P_4 was not **2**, but the tetraphosphidoethyl derivative **8**. Monitoring of the reaction by low-temperature NMR spectroscopy failed to detect any intermediate; this suggests that the insertion of ethene into the Rh–H bond and the subsequent ethyl migration from rhodium to phosphorus is a rapid process. Therefore, a double-insertion process may be reasonably invoked to explain the formation of **8** in place of **2**. In the first reaction step, the metal-promoted intramolecular insertion of C_2H_4 into the Rh–H bond takes place, while in the second elementary step, the rhodium-coordinated ethyl group is selectively conveyed to one of the phosphorus atoms of the activated P_4 molecule. In line with this hypothesis, no reaction takes place when isolated samples of **2** are exposed to an ethene atmosphere. This experiment shows that the insertion of alkene into the Rh–H bond precedes the formation of the P–C bond.

Complexes **7**–**9** are microcrystalline solids with red to orange colour. They slowly decompose in air, but may be stored under nitrogen or argon without decomposition for several days. They are soluble in THF, dichloromethane and acetone, with slow decomposition at temperatures higher than 10 °C. The decomposition is accelerated at room temperature and is fast at 40 °C, resulting in the formation of the cyclotriphosphorus complex **3** in almost quantitative yield (based on the amount of rhodium).

Electrophilic alkylation of [(triphos)Rh(η^1:η^2-P_4R)] complexes: Transition metal complexes containing naked phosphorus atoms or P_x units can be used either to coordinate to electrophilic transition metal centres[34] or to bind to organic electrophiles[35] through the phosphorus lone pair. Therefore, the rhodium-coordinated η^1:η^2-P_4R ligand in the complexes **2**, **7**–**9**, can also be expected to have some reactivity towards electrophilic reagents. Accordingly, treatment of a solution of [(triphos)Rh(η^1:η^2-P_4R)] (R = H (**2**), Ph (**9**)) in THF at −78 °C with one equivalent of MeOTf (OTf = $OSO_2CF_3^-$) under nitrogen resulted in the immediate, quantitative formation of the compounds [(triphos)Rh(η^1:η^2-P_4RR′)]OTf (R′ = Me; R = H (**11**), Ph (**12**)] (see Scheme 5).

Transfer of the methyl carbocation to the already substituted phosphorus atom of the η^1:η^2-P_4R ligand appears to be selective. The course of the alkylation reaction does not

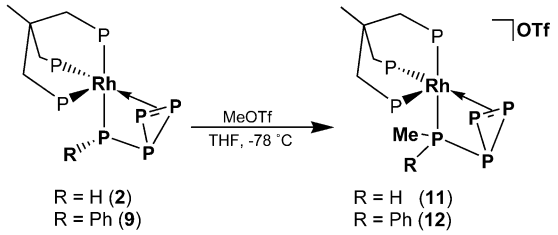

Scheme 5.

change when MeOTf is replaced with the softer electrophile CH_3I, for both **2** and **9**. A metathetical reaction occurs when an excess (2–3 equivalents) of $NaBF_4$, NH_4PF_6 or $NaBPh_4$ in ethanol is mixed with a solution of **12** in THF. This provides a simple method of generating the corresponding tetrafluoroborate, hexafluorophosphate or tetraphenylborate salts [(triphos)Rh(η^1:η^2-P_4PhMe)]Y (Y = BF_4, PF_6, BPh_4) in quantitative yield.

Complexes **11** and **12** are yellowish orange microcrystalline compounds highly sensitive to air in the solid state and in solution. They are highly soluble in polar solvents, such as THF, acetone and chlorinated hydrocarbons, and yield orange solutions that slowly decompose even when maintained under an inert atmosphere at low temperature. The decomposition is almost complete after about 48 h at $-18\,^{\circ}C$ and results in the formation of several phosphorus-containing products including [(triphos)Rh(η^3-P_3)]. In dichloromethane, compound **12** behaves as a typical 1:1 electrolyte. A slow decomposition also takes place in the solid state at room temperature, but the compound can be stored under argon at $-20\,^{\circ}C$ for several weeks without significant decomposition. Moreover, in this case, [(triphos)Rh(η^3-P_3)] is produced together with a complex mixture of compounds; this precludes simple characterisation (NMR/GC-MS analysis). Apart from elemental analyses, **12** was characterised in the solid state by mass spectrometry. The MS analysis confirmed the intrinsic instability of this class of complexes, and a peak corresponding to the mass of the complex cation could not be detected. Indeed, the major fragmentation pathway involves loss of a $PPhMe^+$ fragment (27.9%) to generate the cation [(triphos)Rh(η^3-P_3)]$^+$ appearing as the primary peak of the spectrum.

Structural assignment of **11** and **12** comes from a perusal of the spectral data, particularly from 2D -NMR spectroscopy (^{1}H COSY, ^{1}H NOESY, and ^{1}H,^{31}P/^{1}H,^{13}C correlations, vide infra). The structural features of the present family of [(triphos)Rh(η^1:η^2-P_4RR′)]$^+$ complexes was also confirmed by an X-ray crystallographic study carried out for the phenyl/methyl derivative **12**. A single yellow-orange crystal of **12** suitable for an X-ray diffraction analysis was obtained by slow evaporation of a dichloromethane solution of **12**. X-ray data were collected at 20 °C under conditions detailed in Table 1, and further summarised in the Experimental Section. Twinning and problems of disorder affecting mainly the position of the triflate counter anion were encountered (see Experimental Section). Although the overall quality of the present structure is not optimal, and the metric parameters have to be discussed with caution, the general trends are meaningful and fully supported by the model structure optimised by the DFT method (vide infra).

The ORTEP diagram shown in Figure 1 illustrates the approximate octahedral geometry about the rhodium centre with three *fac* coordination positions occupied by the phosphorus atoms of triphos and the other three by three

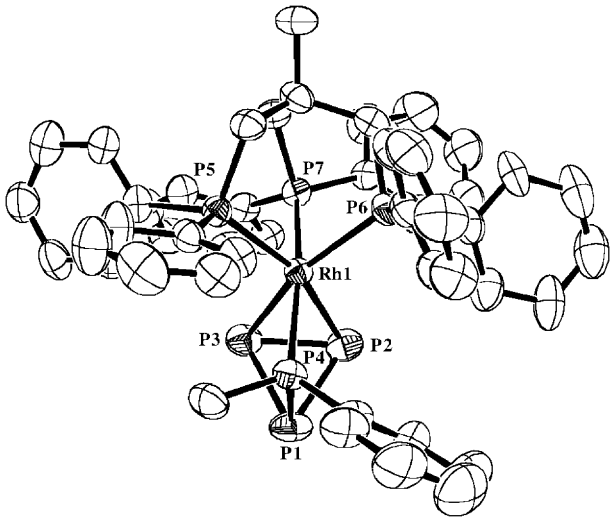

Figure 1. ORTEP drawing of the complex cation [(triphos)Rh(η^1:η^2-P_4PhMe)]$^+$ of **12**·2CH_2Cl_2 (50% probability ellipsoids).

phosphorus atoms of the η^1:η^2-P_4PhMe ligand. In keeping with the NMR analysis, the doubly functionalised phosphorus atom P4, which bears the aryl and alkyl substituents, acts essentially as a fourth phosphine ligand. In this respect, notice that all four distances from Rh to the P atoms numbered from 4 to 7 have a narrow range (2.351(2)–2.373(2) Å). The residual *cyclo*-triphosphorus unit features an uncoordinated P atom, (P1), while the other two atoms, in the equatorial plane, are involved in a η^2-type coordination and are in somewhat similar position to that assumed by ethene in the precursor **10**. Significantly, the corresponding Rh–P2 and Rh–P3 bonds (2.449(1) and 2.441(2) Å) are the longest of this type in the structure.

It is interesting to compare the lengths of the remaining four P–P bonds in the η^1:η^2-P_4PhMe ligand with that in the free P_4 tetrahedron ($d_{(P\text{-}P)ave}$ = 2.21 Å)[36] or with that of the η^3-coordinated *cyclo*-triphosphorus unit in the known structure of complex **3** (2.15 Å).[24, 37] In spite of the three distinct typologies of the P_4-skeleton atoms in **2**, variations in distances are not great; this suggests significant bonding delocalisation over the whole unit. Thus, the P1–P4 bond, which should be the closest to a single bond (because of the evident phosphine character at P1), is less elongated (2.165(2) Å) than those are found for the P1–P2 and P1–P3 bonds within the P_3 ring (2.237(3) Å, average). Furthermore, the most shortened P–P bond is the dihapto coordinated one, namely P2–P3, which has a length of 2.123(3) Å. This suggests a fraction of P=P double bond character at the coordinated bond of the P_3 ring. Some elongation may be consistent with metal back-donation and with an overall strained σ-bonding network in three-membered cycles. Remarkably, the P=P double bond observed in diphosphorus, such as that in $(Me_3Si)_3CP{=}PC(Me_3Si)_3$,[38] is about 0.1 Å shorter than in **12**

(2.015 Å]. On the other hand, diphosphene complexes such as $(PPh_3)_2Pd\{\eta^2\text{-}(CF_3)P{=}P(CF_3)\}$[39] and other known $L_nM\{\eta^2\text{-}RP{=}PR\}$ complexes have P–P separations very similar to those observed in **12**. If metal back-donation is certainly active in all of the previously mentioned species, the full oxidative addition of the P–P linkage featured by η^2-P_4 adducts,[38] can be excluded for **12** in view of the rather long Rh–P bonds. Consequently, the most reasonable oxidation state of the metal is +1, and the $\eta^1{:}\eta^2$-P_4PhMe ligand is a neutral four-electron donor. The bonding description outlined in Scheme 2 for the parent complex **2** is unchanged by electrophilic attack.

The ascertained structure of the complexes **11** and **12** could not be a priori taken for granted as, in principle, all four phosphorus atoms of the $\eta^1{:}\eta^2$-P_4R ligand in the precursors **2** or **9** could be the target of the incoming electrophile. The low-temperature NMR study of the reaction between [(triphos)Rh($\eta^1{:}\eta^2$-P_4R)] and MeOTf shows full regioselectivity of the electrophilic attack. In fact, only the phosphorus atom that already holds the R substituent (R = H, Ph) undergoes a significant downfield shift upon addition of methyltriflate (vide infra NMR section).

The selective attack on the substituted phosphorus atom was unambiguously confirmed by cross experiments carried out singly on the compounds [(triphos)Rh($\eta^1{:}\eta^2$-P_4H)] (**2**) and [(triphos)Rh($\eta^1{:}\eta^2$-P_4Me)] (**7**). Thus, when a sample of **2**, dissolved in CD_2Cl_2 and cooled to −78 °C in a 5 mm screw-cap NMR tube, is treated with one equivalent of MeOTf, the ^{31}P NMR spectrum is unambiguous: the alkylated complex [(triphos)Rh($\eta^1{:}\eta^2$-P_4HMe)]$^+$ is quickly and selectively formed in quantitative yields. Under the same experimental conditions, the addition of $HBF_4 \cdot OMe_2$ to a cooled solution of **7** generates the same product **11** in quantitative yields. In conclusion, the attack of an electrophile appears to be regioselectively directed to the monosubstituted P-atom. For convenience, Scheme 6 highlights the formation of a unique product (**11**) from the electrophilic attacks on either **2** or **7**, and illustrates the alternative paths that could be expected but which were not observed.

Solution structure of [(triphos)Rh($\eta^1{:}\eta^2$-P_4R)] and [(triphos)Rh($\eta^1{:}\eta^2$-P_4RR′)]Y complexes by NMR spectroscopy: The solution structure of complexes [(triphos)Rh($\eta^1{:}\eta^2$-P_4R)] (R = H (**2**), Me (**7**), Et (**8**), Ph (**9**)) and [(triphos)Rh($\eta^1{:}\eta^2$-P_4RR′)]Y (R = H, R′ = Me (**11**), Y = OTf, BF_4; R = Ph, R′ = Me (**12**), Y = OTf] was determined by using multinuclear, multidimensional NMR spectroscopy. For the sake of clarity, a sketch of the compounds examined, together with the labelling scheme adopted for NMR assignments is shown in Figure 2, while detailed $^{31}P\{^1H\}$, ^1H and $^{13}C\{^1H\}$ NMR data for the rhodium(I) complexes are listed below in Tables 3–5, respectively.

It is noteworthy that the neutral Rh-$\eta^1{:}\eta^2$-P_4R and the cationic Rh-$\eta^1{:}\eta^2$-P_4RR′ complexes show a strictly similar NMR behaviour. This indicated that the stereochemistry of the whole system is barely affected by the presence of a lone pair at the coordinating PR group (neutral complex) or by the additional R′ substituent (cation), and confirms that the bonding description of **2** can also reasonably be applied to the alkylated complexes **11** and **12**.

In each complex, all the ^{31}P, ^{1}H and ^{13}C nuclei are chemically nonequivalent, because of the lack of any symmetry in the molecule. Only the triphos methyl protons as well as those of the *ortho* and *meta* pairs on the same phenyl group become equivalent on account of the fast rotation around the C–C and C–P bonds, respectively. The A, B and C phosphorus nuclei of triphos were labelled as the ones *trans* to the E, F and D

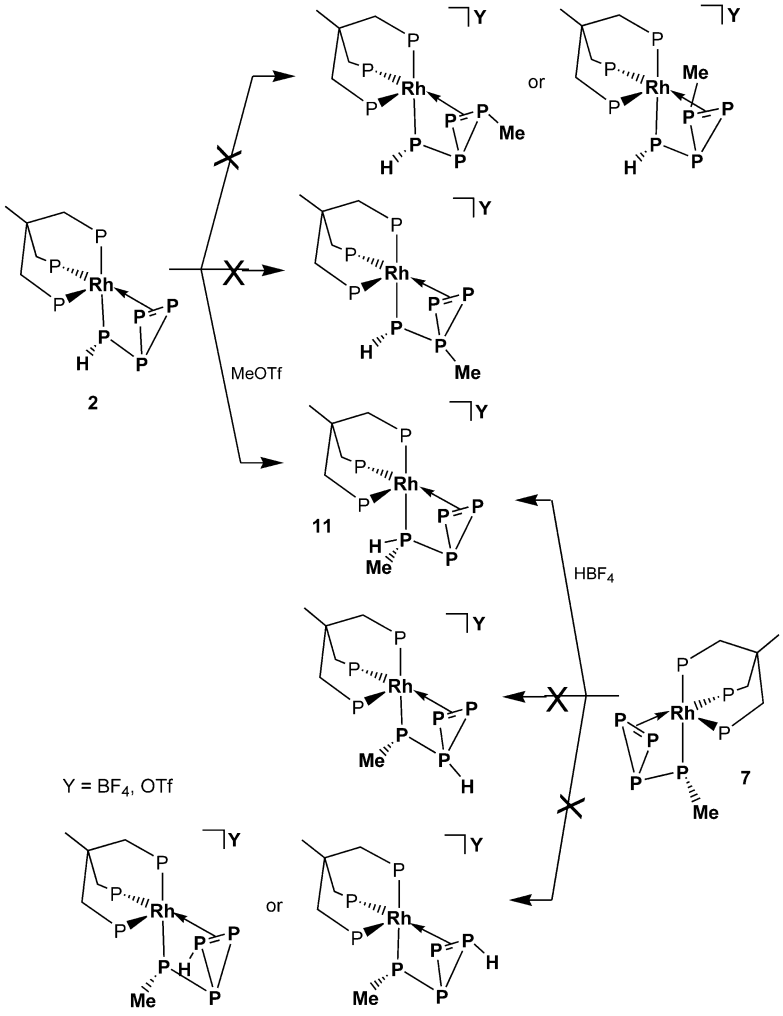

Scheme 6.

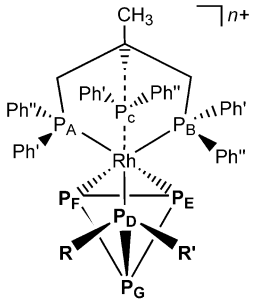

2 R = H, R' = 2e$^-$, n = 0 [(triphos)Rh(η^1,η^2-P_4H)]

7 R = Me, R' = 2e$^-$, n = 0 [(triphos)Rh(η^1,η^2-P_4Me)]

8 R = Et, R' = 2e$^-$, n = 0 [(triphos)Rh(η^1,η^2-P_4Et)]

9 R = Ph, R' = 2e$^-$, n = 0 [(triphos)Rh(η^1,η^2-P_4Ph)]

11 R = Me, R' = H, n = 1 [(triphos)Rh(η^1,η^2-P_4MeH)]$^+$

12 R = Ph, R' = Me, n = 1 [(triphos)Rh(η^1,η^2-P_4PhMe)]$^+$

Figure 2. Sketch of the [(triphos)Rh(η^1:η^2-P_4RR′)]Y complexes showing the labelling scheme adopted for the NMR assignments.

phosphorus nuclei of the P_4RR′ unit, respectively. A higher chemical shift relative to P_B was arbitrarily assigned to P_A.

For each complex, all the NMR resonances were unambiguously assigned by a combination of 1D and 2D NMR techniques (see Experimental Section). The ^{31}P NMR signals, which form a seven-resonance ABCDEFGX spin system (X = ^{103}Rh), were easily assigned on the basis of the ^{31}P{^{1}H} COSY spectra. An illustrative section of the ^{31}P{^{1}H} COSY spectrum of [(triphos)Rh(η^1:η^2-P_4Ph)] (**9**) is reported in Figure 3 as an example. The network of resonances belonging to the phosphorus nuclei of the P_4RR′ ligand was unambiguously identified by the characteristic three strong $^1J_{PP}$ couplings between the P_G atom and P_D, P_E and P_F, as well as by the strong $^1J_{PP}$ cross-peak connecting P_E and P_F.[40]

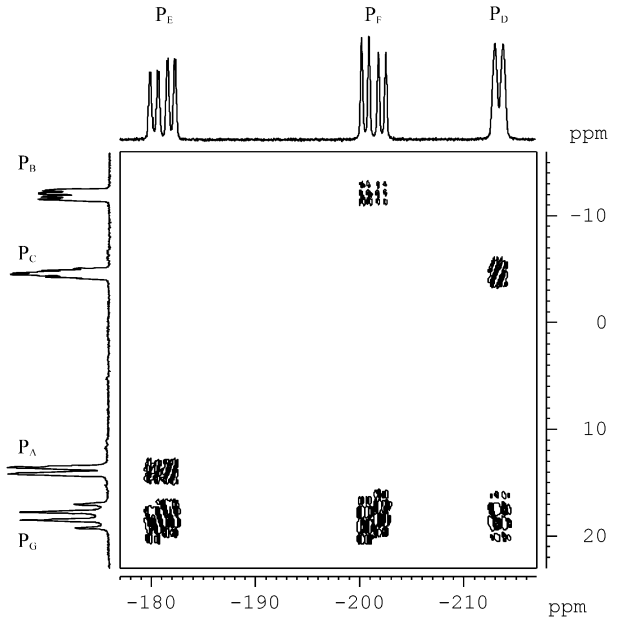

Figure 3. Section of the ^{31}P{^{1}H} COSY spectrum of [(triphos)Rh(η^1:η^2-P_4Ph)] (**9**) (202.47 MHz, [D_8]THF, 266 K). Strong cross-peaks due to the $^1J_{PP}$ couplings between the phosphorus atom of triphos are observed, as well as medium-intensity peaks connecting the P_A–P_E, P_B–P_F and P_C–P_D couples of nuclei in *trans* position.

A perusal of the COSY spectra also allowed us to assign the resonances due to the phosphorus nuclei of triphos. In fact, the observed medium-intensity cross-peaks to the nuclei of the P_4RR′ moiety were ascribed to a $^2J_{PP}$ *trans* coupling.[40–42] Small to medium $^2J_{PP}$ cross-peaks, which connect the three phosphorus donor atoms of triphos, were also observed and facilitated the assignment.

The above attributions were supported by the values of the J_{PP} coupling constants, which were determined by computer simulation of the ^{31}P{^{1}H} NMR spectra (Table 3).[17] As a paradigmatic example, both the computed and experimental ^{31}P{^{1}H} NMR spectra of **12** are reported in Figure 4. Indeed, $^1J_{P_DP_G}$, $^1J_{P_EP_G}$ and $^1J_{P_FP_G}$ couplings in the range 111.3–169.0 Hz and $^1J_{P_EP_F}$ couplings of about 325.0 Hz were observed for the nuclei of the P_4RR′ units. $^1J_{PP}$ couplings of such magnitude are particularly large and unusual for single P–P bonds.[7] In contrast, values greater than 250 Hz have been reported for transition-metal complexes bearing η^2-diphosphenes li-

Table 3. ^{31}P{^{1}H} NMR data for [(triphos)Rh(η^1:η^2-P_4RR′]Y complexes.[a]

	Complex					
	2[b]	**7**[b]	**8**[c]	**9**[d]	**11**[c]	**12**[e,f]
δ (ppm)						
P_A	15.96	15.61	12.49	13.86	15.88	15.91
P_B	2.81	−1.94	−2.44	−12.03	9.75	2.56
P_C	−10.78	−11.77	−11.42	−4.63	5.21	9.46
P_D	−280.22	−214.08	−192.91	−213.44	−172.02	−156.75
P_E	−180.12	−174.52	−178.24	−181.09	−190.11	−200.77
P_F	−184.98	−198.79	−199.92	−201.39	−209.25	−174.04
P_G	−3.33	26.79	24.28	18.14	5.60	17.39
J [Hz]						
P_A P_B	12.5	16.9	14.5	14.5	13.1	13.0
P_A P_C	31.6	31.9	31.5	32.1	35.0	32.1
P_A P_D	19.1	7.0	6.0	17.0	0.0	1.0
P_A P_E	28.3	24.8	26.5	27.0	18.2	23.2
P_A P_F	3.1	0.0	5.3	5.0	9.1	16.0
P_A P_G	7.1	0.0	4.3	5.0	0.0	0.0
P_B P_C	40.0	54.3	54.1	55.0	40.1	42.0
P_B P_D	6.4	0.0	0.0	4.0	0.0	4.0
P_B P_E	5.4	18.3	24.8	22.0	0.0	13.3
P_B P_F	5.4	18.3	24.8	17.0	13.1	18.9
P_B P_G	7.1	0.0	4.3	2.0	0.0	0.0
P_C P_D	50.2	23.9	26.8	29.3	379.0	383.0
P_C P_E	0.0	0.0	0.0	2.0	0.0	10.0
P_C P_F	0.0	0.0	0.0	2.0	0.0	2.0
P_C P_G	7.1	13.5	13.7	12.2	0.0	0.0
P_D P_E	24.4	20.1	19.3	23.0	0.0	2.0
P_D P_F	24.4	20.1	19.3	23.0	0.0	11.1
P_D P_G	119.5	138.0	152.4	160.8	169.0	166.6
P_E P_F	321.9	327.4	327.5	327.1	332.2	329.4
P_E P_G	144.5	150.5	152.1	145.4	144.0	122.7
P_F P_G	155.0	150.5	152.1	145.4	111.3	119.3
P_A Rh	121.1	122.7	121.9	121.5	106.2	117.1
P_B Rh	112.5	116.3	116.7	116.0	108.2	104.5
P_C Rh	78.8	73.5	74.6	78.1	79.0	83.0
P_D Rh	42.2	49.5	49.2	49.9	79.0	81.4
P_E Rh	20.0	0.0	0.0	4.0	16.0	17.5
P_F Rh	20.0	0.0	0.0	4.0	25.0	32.0
P_G Rh	7.0	6.5	4.3	6.0	0.0	0.0

[a] 202.46 MHz, [D_8]THF. Data from computer simulation. [b] 293 K. [c] 253 K. [d] 266 K. [e] CD_2Cl_2. [f] 275 K.

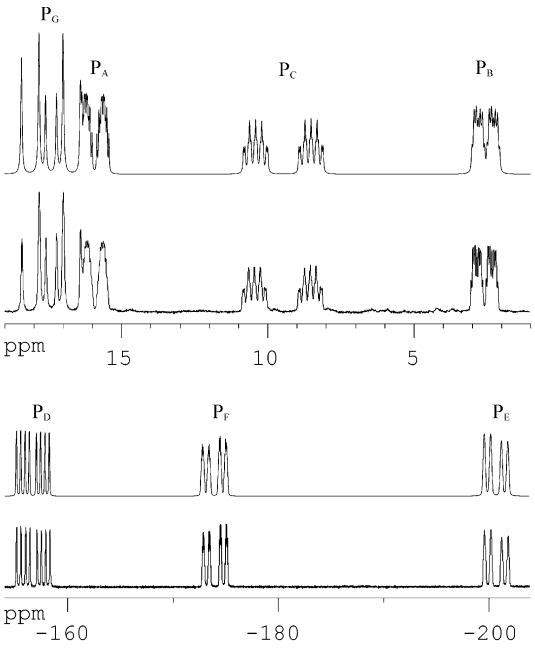

Figure 4. Sections of the simulated (above) and experimental (below) $^{31}P\{^1H\}$ NMR spectra of [(triphos)Rh(η^1:η^2-P_4PhMe)]$^+$OTf (**12**) recorded at 273 K (CD_2Cl_2, 202.47 MHz).

gands.[43] The hypothesis is supported by the P_E–P_F separation of 2.123(3) Å, experimentally determined in **12** by X-ray methods. The distance is definitely shorter than typical P–P single bond lengths,[2, 44] and underpins the theoretical arguments discussed below.

Consistent with a *trans* arrangement, the $^2J_{P_AP_E}$ couplings (18.2–28.3 Hz) are greater than $^2J_{P_AP_F}$ (0.0–16.0 Hz) and $^2J_{P_AP_D}$ (1.0–19.1 Hz) in each compound. In keeping with the assumed stereochemical arrangement shown in Figure 2, the $^2J_{P_CP_D}$ constants (23.9–383.0 Hz) exceed $^2J_{P_CP_E}$ (0.0–10.0 Hz) and $^2J_{P_CP_F}$ (0.0–2.0 Hz) in all complexes.[40–42] The small values of the $^1J_{P_CRh}$ constants (73.5–83.0 Hz), compared with $^1J_{P_ARh}$ (106.2–122.7 Hz) and $^1J_{P_BRh}$ (104.5–116.7 Hz), are in line with the ^{31}P assignments, and can be rationalised in terms of the *trans* influence of the P_DRR' group.[42, 45–47]

The ^1H NMR signals of triphos were assigned straightforwardly on the basis of 1D and 2D NMR spectra (Table 4). The ^1H resonances due to P_DRR' group in [(triphos)Rh(η^1:η^2-P_4RR')]Y could be unambiguously assigned only through a ^1H,^{31}P correlation that was optimised for the detection of small J_{HP} scalar couplings (ca. 5 Hz).[48] A section of the ^1H,^{31}P correlation of [(triphos)Rh(η^1:η^2-P_4Ph)], tuned for a J_{HP} coupling of 5 Hz, is reported in Figure 5.[49]

As a matter of fact, the values of $^2J_{HP_D}$ and $^3J_{HP_D}$, which are as small as 5 Hz or less, were measured for the $P_DR(R')$ protons (Table 4) in complexes **7**–**9** and **11**–**12**. Thus, 1D $^1H\{^{31}P\}$-selective decoupled spectra often resulted only in the removal of couplings that were far below the experimental line width (as for **9**). In a few cases, the ^1H,^{31}P correlations even allowed the detection of long-range J_{HP} couplings. An example section of the ^1H,^{31}P correlation of [(triphos)Rh(η^1:η^2-P_4PhMe)]OTf (**12**) in the P_DCH_3 region is reported in Figure 6.

Table 4. Selected ^1H NMR data for the [(triphos)Rh(η^1:η^2-P_4RR']Y Complexes.[a]

Complex	Proton assignment	δ (ppm)	J [Hz]
2[b]	P_DH	0.01 (br dd)	$^2J_{HP}$ 28.3, $^1J_{HP}$ 119.9
7[b]	P_DCH_3 (3H)	0.65 (br s)	
8[c]	$P_DCH_2CH_3$ (3H)	0.70 (q)	$^3J_{HH}=^3J_{HP}=7.9$
	P_DCH'	1.42 (m)	$^3J_{HH}=7.5$, $^2J_{HH}=13.3$, $^2J_{HP}=7.3$
	P_DCH''	0.30 (m)	$^3J_{HH}=8.3$, $^2J_{HH}=13.3$, $^2J_{HP}=6.3$
9[d]	*o*-PhP_D (2H)	7.66 (br d)	$J_{HH}=7.0$
	m-PhP_D (2H)	6.50 (t)	$J_{HH}=7.7$
	p-PhP_D (2H)	6.60 (t)	$J_{HH}=7.2$
	o-Ph′P_A (2H)	5.71 (t)	8.5
	o-Ph″P_A (2H)	8.12 (t)	8.6
	o-Ph′P_B (2H)	8.48 (t)	8.4
	o-Ph″P_B (2H)	8.09 (t)	7.8
	o-Ph′P_C (2H)	6.47 (t)	8.1
	o-Ph″P_C (2H)	7.33 (t)	8.6
11[d]	P_DCH_3 (3H)	0.82 (br s)	
	P_DH	3.50 (br d)	$^1J_{HP}$ 256.0
12[e,f]	P_DCH_3 (3H)	0.93 (br d)	$^2J_{HP}=7.7$
	o-PhP_D (2H)	8.01 (t)	$^3J_{HH}=^3J_{HP}$ 5.6
	m-PhP_D (2H)	7.65[g]	
	p-PhP_D(2H)	6.98[g]	
	o-Ph′P_A (2H)	6.23 (dd)	7.9, 11.1
	o-Ph″P_A (2H)	8.50 (t)	8.7
	o-Ph′P_B (2H)	8.21 (br)	
	o-Ph″P_B (2H)	6.66 (t)	9.4
	o-Ph′P_C (2H)	6.06 (t)	9.7
	o-Ph″P_C (2H)	7.49 (t)	9.0

[a] 500.132 MHz, [D_8]THF; unresolved multiplet unless otherwise specified. [b] 293 K. [c] 253 K. [d] 266 K. [e] CD_2Cl_2. [f] 275 K. [g] Partially masked by other resonances.

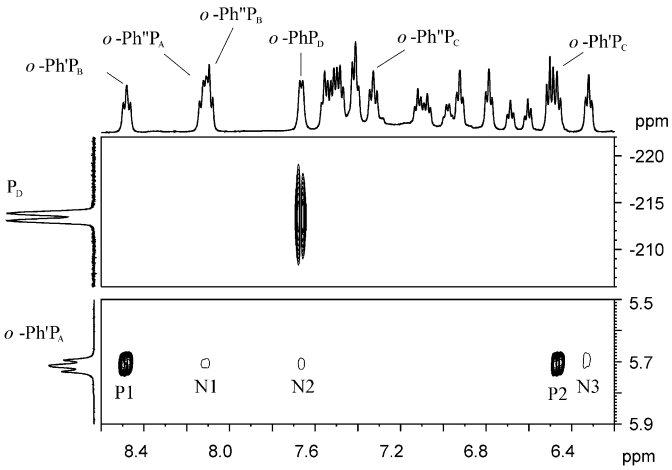

Figure 5. Sections of 2D NMR spectra of [(triphos)Rh(η^1:η^2-P_4Ph)] (**9**) (500.13 MHz, [D_8]THF, 266 K). Top: ^1H–^{31}P correlation, bottom: ^1H NOESY ($\eta_{lm}=1.0$ s), positive-phased (exchange) cross-peaks (●), negative-phased (NOE) cross-peaks (○). Labels: N1 (*o*-Ph′P_A–*o*-Ph″P_A), N2 (*o*-Ph′P_A–*o*-PhP_D), N3 (*o*-Ph′P_A–*m*-Ph′P_A).[49]

Although the P_DCH_3 resonance appeared as a broad doublet in the ^1H NMR spectrum (a value of $^2J_{HPD}=7.7$ Hz was measured from an $^1H\{^{31}P\}_{PD}$-selective decoupling experiment), $^3J_{HP}$ and $^4J_{HP}$ couplings to P_G, P_E and P_C are also evident in the 2D spectrum of Figure 6. Analogously, the two diastereotopic methylenic protons of the $P_DCH_2CH_3$ moiety in [(triphos)Rh(η^1:η^2-P_4Et)] (**8**) appear as two complex multiplets at 1.42 and 0.30 ppm, which correspond to $^2J_{HP_DD}$

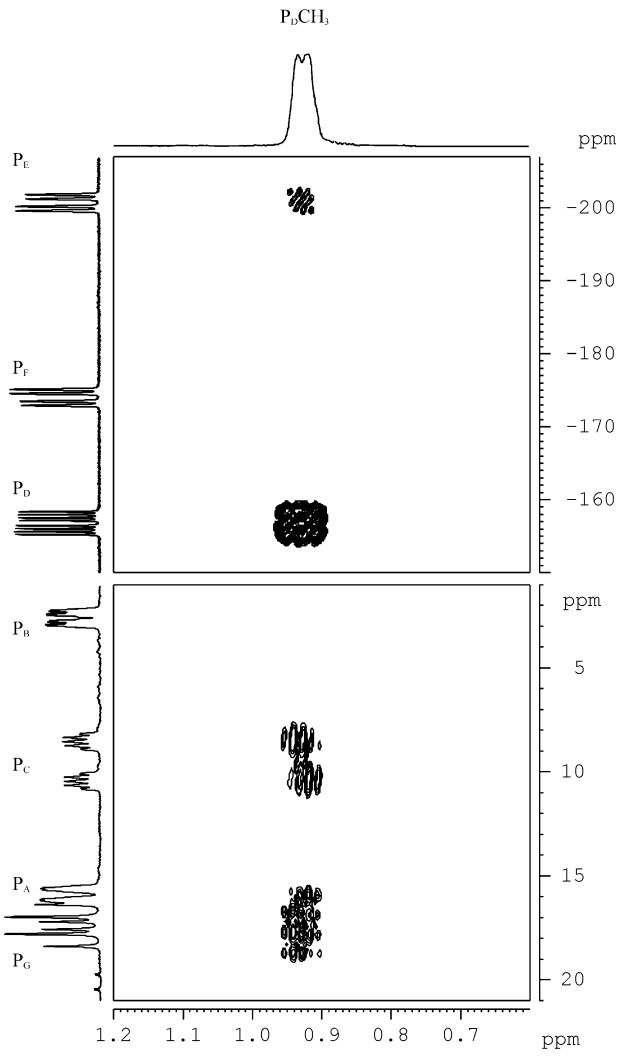

Figure 6. Section of the 2D $^{1}H-^{31}P$ HMQC correlation of [(triphos)Rh(η^1:η^2-P_4PhMe)]OTf (**12**) (500.13 MHz, CD_2Cl_2, 275 K) in the P_DCH_3 region.

values of 7.3 and 6.3 Hz, respectively. The latter magnitudes were measured from selective $^{1}H\{^{31}P\}$ decoupling experiments together with residual couplings to P_C and P_G. A series of $^{1}H,^{31}P$ NMR correlations optimised for J_{HP} values of about 120 Hz was needed to detect the P_D–H coupling in **2** and **11** (R = H). $^{1}J_{HP_D}$ values of 119.9 and 353.0 Hz were measured for the hydride complexes in both the neutral [(triphos)Rh(η^1:η^2-P_4H)] (**2**) and the cationic [(triphos)Rh(η^1:η^2-P_4MeH)]$^+$ (**11**) species, respectively.

Detailed assignments of ^{13}C NMR resonances for each complex were possible on the basis of both HMQC and HMBC $^{1}H,^{13}C$ correlations. Selected $^{13}C\{^{1}H\}$ NMR data for [(triphos)Rh(η^1:η^2-P_4R)] (R = H (**2**), Me (**7**), Et (**8**), Ph (**9**)) and [(triphos)Rh(η^1:η^2-P_4RR′)]Y (R = H, R′ = Me (**11**); R = Ph, R′ = Me (**12**)) are reported in Table 5. A section of the $^{1}H,^{13}C$ correlation in the methyl region of [(triphos)Rh(η^1:η^2-P_4PhMe)]OTf (**12**) is reported in Figure 7.

All of the resonances pertaining to the R(R′) carbons show phosphorus couplings in the $^{13}C\{^{1}H\}$ NMR spectra. A series of $^{13}C\{^{1}H\}\{^{31}P\}_{sel}$ experiments was carried out as useful probes for the unambiguous assignment of the R(R′) substituents on the

Table 5. Selected $^{13}C\{^{1}H\}$ NMR data for the [(triphos)Rh(η^1:η^2-P_4RR′]Y complexes.[a]

Complex	Carbon assignment	δ (ppm)	J [Hz]
7[b]	P_DCH_3	14.59 (br d)	$^{1}J_{CP}$ 18.8
8[c]	P_DCH_2	31.43 (d)	$^{1}J_{CP}$ 45.3
	$P_DCH_2CH_3$	13.33 (s)	
9[d]	*i*-PhP_D	151.45 (br d)	$^{1}J_{CP}$ 71.4
	o-PhP_D	137.55 (br d)	$^{2}J_{CP}$ 12.6
	m-PhP_D	127.79 (s)	
	p-PhP_D	127.06 (s)	
	o-Ph′P_A	133.87 (d)	$^{2}J_{CP}$ 10.8
	o-Ph″P_A	135.96 (t)	$^{2}J_{CP}$ 9.4
	o-Ph′P_B	134.25[g]	
	o-Ph″P_B	134.31[g]	
	o-Ph′P_C	133.49 (br d)	$^{2}J_{CP}$ 5.1
	o-Ph″P_C	136.43 (t)	$^{2}J_{CP}$ 10.3
11[d]	P_DCH_3	11.37 (br d)	$^{1}J_{CP}$ 14.7
12[e,f]	P_DCH_3	19.70 (br)	$^{1}J_{CP}$ 21.1
	o-PhP_D	133.22 (d)	$^{2}J_{CP}$ 6.8
	o-Ph′P_A	132.45 (d)	$^{2}J_{CP}$ 11.6
	o-Ph″P_A	133.68 (br)	
	o-Ph′P_B	132.34[g]	
	o-Ph″P_B	131.23 (d)	$^{2}J_{CP}$ 8.9
	o-Ph′P_C	132.73[g]	
	o-Ph″P_C	134.28 (t)	$^{2}J_{CP}$ 10.9

[a] 125.76 MHz, $[D_8]$THF. [b] 293 K. [c] 253 K. [d] 266 K. [e] CD_2Cl_2. [f] 275 K. [g] Partially masked by other resonances.

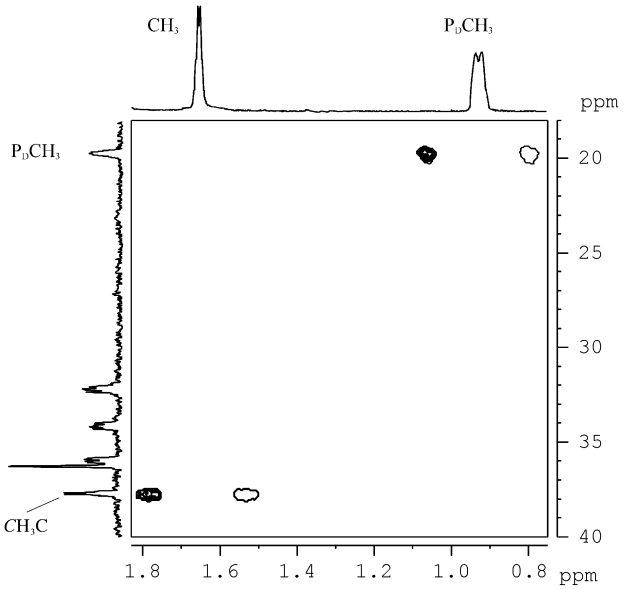

Figure 7. Section of the 2D $^{1}H-^{13}C$ HMQC correlation of [(triphos)Rh(η^1:η^2-P_4PhMe)]OTf (**12**) (500.13 MHz, CD_2Cl_2, 275 K) in the methyl region. The spectrum was recorded with no decoupling during acquisition. $^{1}J_{HC}$ coupling constants are apparent on *F*2.

P_D phosphorus atom. The $^{13}C\{^{1}H\}\{^{31}P\}$ NMR traces of [(triphos)Rh(η^1:η^2-P_4PhMe)]OTf in the P_DCH_3 and *ortho*-PhP_D regions are reported in Figure 8 as an illustrative example.

The P_DCH_3 and the *ortho*-PhP_D $^{13}C\{^{1}H\}$ resonances appeared as an unresolved multiplet and a doublet, respectively (trace a). A selective $^{13}C\{^{1}H\}\{^{31}P\}_{P_D}$ experiment (trace b) proved the *ortho*-PhP_D carbons to be coupled to P_D with a $^{2}J_{CP_D}$ constant of 6.8 Hz. Also, from a comparison with the

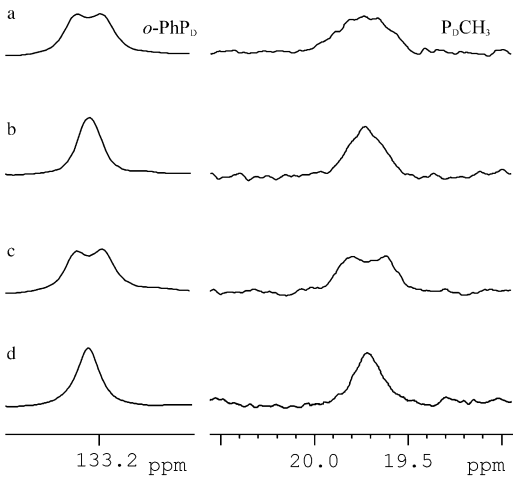

Figure 8. Sections of the ^{13}C NMR spectra of [(triphos)Rh(η^1:η^2-P_4PhMe)]OTf (**12**) (125.76 MHz, CD_2Cl_2, 275 K) in the P_DCH_3 (right) and *o*-PhP_D (left) region. a) $^{13}C\{^1H\}$ spectrum, b) $^{13}C\{^1H\}\{^{31}P\}$ spectrum selectively decoupled from the P_D signal, c) $^{13}C\{^1H\}\{^{31}P\}$ spectrum selectively decoupled from the P_G signal, d) $^{13}C\{^1H\}\{^{31}P\}$ spectrum recorded with ^{31}P unselective decoupling.

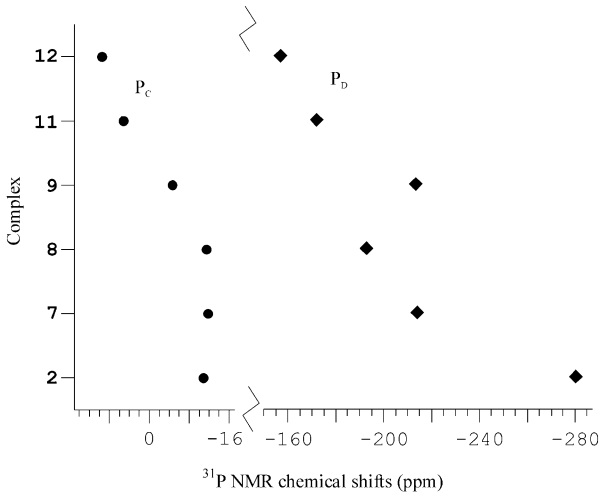

Figure 9. Observed ^{31}P chemical shift (ppm) of the P_C and P_D nuclei in the complexes [(triphos)Rh(η^1:η^2-P_4R)] (R = H (**2**), Me (**7**), Et (**8**), Ph (**9**)) and [(triphos)Rh(η^1:η^2-P_4RR′)]Y (R = H, R′ = Me (**11**); R = Ph, R′ = Me (**12**)).

corresponding broadband-decoupled spectrum (trace d), a residual coupling to other phosphorus nuclei could be envisaged for the P_DCH_3 carbon. Indeed, a $^1J_{CP_D}$ constant of 21.1 Hz could be measured for the P_DCH_3 carbon from a selective $^{13}C\{^1H\}\{^{31}P\}_{PG}$ experiment (trace c).

^1H NOESY experiments carried out on both [(triphos)Rh(η^1:η^2-P_4R)] and [(triphos)Rh(η^1:η^2-P_4RR′)]Y complexes showed that the *extreme narrowing limit* ($\tau_c\omega_L \ll 1$) is attained by each complex in our experimental conditions and, thus, only positive (negative-phased) NOEs are displayed (except for **11**, [D_8]THF solution, 253 K).[19, 50] A section of the ^1H NOESY spectrum of [(triphos)Rh(η^1:η^2-P_4Ph)] (**9**) is reported in Figure 4. The observed NOE between the *ortho*-Ph′P_A and the *ortho*-PhP_D protons indicates that the PhP_D aromatic ring faces the Ph′P_A phenyl (see Figure 2). This finding may also explain the unusual low-frequency chemical shift observed for the *ortho*-Ph′P_A protons (5.71 ppm), probably due to the shielding effect of the PhP_D ring. The arrangement of the P_4R substituents in the compounds [(triphos)Rh(η^1:η^2-P_4R)] (R = H (**2**), Me (**7**), Et (**8**)) and [(triphos)Rh(η^1:η^2-P_4RR′)]Y (R = H, R′ = Me (**11**); R = Ph, R′ = Me (**12**)) was similarly attributed on the basis of the NOESY spectra, as reported in Figure 2.[51]

A general comment can be made for the series of compounds [(triphos)Rh(η^1:η^2-P_4RR′]OTf regarding correlation between the observed ^{31}P NMR chemical shifts and coupling constants and the electronic nature of the R(R′) substituents on the P_D nucleus. As shown in Figure 9, the chemical shift of the P_D nucleus and, to a lesser extent, of its triphos *trans* counterpart P_C is extremely sensitive to the electron-donating properties of the R(R′) groups. Thus, on passing from R = H (**2**, −280.22 ppm), to R = Me (**7**, −214.08 ppm) and to R = Et (**8**, −192.91 ppm), an increasing deshielding effect is observed, whereas an intermediate shift is shown by the π-donor substituent R = Ph (**9**, −213.44 ppm). The introduction of an overall cationic charge on the complex framework causes large downfield shifts of the P_D atoms in the electrophilically alkylated complexes **11** and **12** (R, R′ = Me, H: −172.02 ppm and R, R′ = Ph, Me: −156.75 ppm, respectively).

Finally, it is worth noting the large increase of the $^2J_{P_CP_D}$ coupling constants in the cationic complexes **11** and **12** (379.0 and 383.0 Hz, respectively) with respect to the neutral complexes **2, 7**–**9** (23.9, 50.2 Hz). This is likely to be due to the acquired metal-phosphine character of the Rh–PD bond upon alkylation of the P_D centre (vide infra). In particular, the $^2J_{P_CP_D}$ coupling constants in **11** and **12** approach the values expected for *trans*-disposed phosphine ligands in rhodium complexes.[42] In agreement with this picture, the angle P5-Rh-P4 (165.14(5)°) is the largest one in the solid-state structure of **12**.

DFT computational analysis: The DFT calculations were performed in order to clarify geometrical and energetic aspects of some of the systems illustrated above. The optimised model [(Htriphos)Rh(η^1:η^2-P_4H)] (**2a** reported in Figure 10) is of particular interest, since the molecular

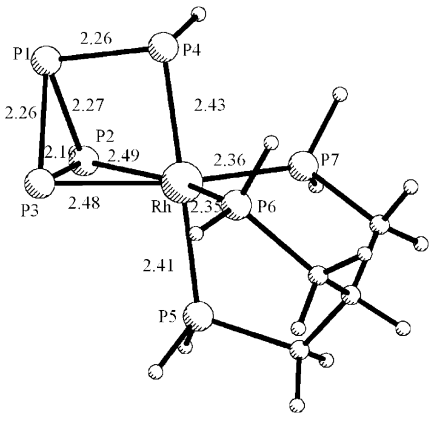

2a

Figure 10. Optimised structure of the model complex [(Htriphos)Rh(η^1:η^2-P_4H)] **2a**. Bond lengths are given in Å.

structure of the actual complex **2** could not be experimentally determined.

There are six P donor atoms coordinated to the metal, although the structure is better described as a trigonal bipyramid rather than a pseudo-octahedron geometry (vide infra). The P atoms of Htripos occupy the *fac* positions, the P_4H may be viewed as a three-membered ring with an exocyclic PH group that is σ-bound to the metal *trans* to the P5 atom of Htriphos (P4-Rh-P5 = 179°). One P–P linkage of the ring, which is opposite the external P–P bond, lies in the plane defined by the metal and the P6 and P7 atoms of Htriphos. In spite of the dihapto coordination to the metal (the Rh–P2 and Rh–P3 lengths of about 2.485 Å are the longest in the structure), the P2–P3 linkage is the shortest (2.16 Å) bond in the P_3 ring. The other two linkages are also long (2.26 Å) and practically equal to the exocyclic P1–P4 bond. Under these circumstances, a significant amount of metal back donation may be operative (as mentioned in the crystallographic section that genuine η^2-coordinated P=P linkages are at least 0.1 Å shorter than in **2a**). However, the oxidative addition of the metal can reasonably be excluded, the ligand being monoanionic (P_4H^-) and the metal being in oxidation state +1 (see below a further discussion of the point). The P4–H linkage is significantly bent (by ca. 78°) with respect to the mirror plane of the P_4 skeleton. Thus, the atom P4 has sp^3 hybridisation; this suggests the presence of a lone pair. A model (**2b**) with the P–H bond in the pseudo-symmetry plane of the P_4H fragment has been optimised as a transition state for the interconvertion involving the pyramidalisation at position P4. The associated energy is about 37 kcal mol^{-1} higher than that of the ground state and excludes an energetically accessible assembly process. This is fully consistent with the solution structure determined by NMR methods, which suggested a fixed orientation of the R substituents in [(triphos)Rh(η^1:η^2-P_4R)] complexes.

Because of its geometrical features and the lack of a rapid inversion process, the lone pair on the P4 atom is the ideal site for an external electrophilic attack. On the other hand, and consistent with the nucleophilic character exhibited by the atoms in metal coordinated P_x units,[34, 35] the other P atoms of P_4H can also be attacked by electrophiles. Unfortunately, the calculated Mulliken as well as the NBO charges[52] of the four P atoms of the unit P_4H in **2a** do not allow a quick identification of the site of the electrophilic attack. We will point out below that the electrophilic attack appears more orbital- than charge controlled.

The energetics of the four alternative products of the protonation at the P_4H fragment have been evaluated computationally and are reported in Table 6. In Figure 11, only the last three isomers are presented. In fact, protonation at the dihapto-coordinated atoms P2 or P3 is only in principle non-equivalent due to the asymmetric orientation of the P4–H bond. Model **13c**, in which the two H atoms both point in one direction, is only about 0.1 kcal mol^{-1} more stable than its stereoisomer. In any event, the two isomers are energetically the least favoured. Actually, models **13a** and **13b** are more stable by 17.8 and 9.64 kcal mol^{-1}, respectively.

Table 6. Calculated total energies [Hartree] and energy differences [kcal mol^{-1}] for the optimised complexes.

Complex	Total energy	E(2a) – E(X)	E(13a) – E(X)
2a	– 2659.92411	0.00	
2b[a]	– 2659.86451	37.4	
13a	– 2660.33118		0.00
13b	– 2660.31581		9.64
13c	– 2660.30271		17.8
13d	– 2660.30277		17.9

[a] Transition state.

Consistent with the experimental findings for the complexes **11** and **12**, the pseudo C_s model **13a** is the most stable. It carries two H substituents at the P4 atom in place of the H/CH_3 and CH_3/Ph pairs. The geometric trends are consistent with those of the X-ray structure of [(triphos)Rh(η^1:η^2-P_4PhMe)]$^+$, **12**. The (Htriphos)Rh fragment matches the experimental analogue almost perfectly (Rh–P bonds in the range 2.35 – 2.38 Å). Concerning, the Rh-(η^1:η^2-P_4H_2) interactions, the weakest Rh–P bonds are confirmed to be those that involve the dihapto-coordinated linkage (P2–P3). However, the experimental lengths are somewhat shorter than the computed ones (2.441(2) and 2.449(2) versus 2.51 Å). Moreover, the trend for the P–P bonds is consistent. Thus, P2–P3 is the shortest bond (2.15 Å), while the exocyclic P1–P4 bond is significantly shorter than the remaining endocyclic linkages (compare the values 2.18 Å and 2.28 Å). This is a consequence of the evident *phosphine* character of the atom P4, which should confer single-bond character on P1–P4.

Compared with the unprotonated precursor **2a**, the most evident effect in **13a** is the shortening of the P4–P1 and Rh–P4 bonds (from 2.26 to 2.18 Å and from 2.41 to 2.35 Å, respectively). The latter effect in particular is in line with a true phosphine character of the P4 donor in **13a**. Most probably, a great portion of the stabilisation of this isomer depends on the increased strength of the Rh–P4 bond itself. In contrast, the well-developed lone pair at the P4 atom in **2a** is probably indicative of electronic repulsion with filled metal orbital(s).

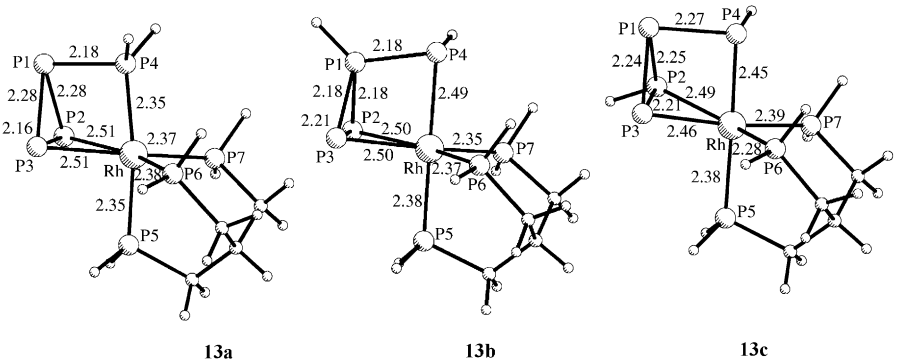

Figure 11. Optimised structure of the model complexes **13a**, **13b**, and **13c**. Bond lengths are given in Å.

It is evident from the geometries of isomers **13b** and **13c** that a second H atom at different sites of the P_4H skeleton allows the primary $\eta^1{:}\eta^2$ bonding mode of the P_4H_2 fragment to be maintained. However, the Rh–P and P–P bonds are affected. Since, in any case, the P4 atom remains with its lone pairs, electronic repulsion elongates the Rh–P4 bond, as in **2a** (>2.44 Å). In **13b**, the geometry of the P_3 ring is significant altered. While the η^2-coordinated P–P linkage elongates by 0.05 Å, the other two bonds shrink from 2.28 to 2.18 Å. In **13c**, the latter trend is reversed again. In this case, the η^2-coordinated P–P linkage is forced to be asymmetric with evident distortional effects on the geometry of the whole P_4H_2 ligand.

In order to provide a qualitative MO explanation of the electron distribution and stability of **13a**, the nature of the four highest occupied MOs in the precursor **2a** was analysed. The picture that emerges from the EHMO calculations is consistent with that of the DFT calculations and, for the sake of clarity, the illustration will be based on the former method. The MOs mentioned are relatively close in energy and, while three of them are clearly metal nonbonding ("t_{2g}"-like levels), the fourth level, illustrated in Figure 12, combines a double

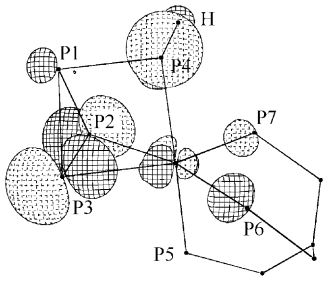

Figure 12. The fourth HOMO of the precursor **2a** (EHMO level) shows a well-developed lone pair at the P4 atom.

functionality. Namely, it has a well-developed lone-pair character at the P4 atom and it also has d_π/π^* bonding character between the metal and the in-plane P=P linkage. In other words, a significant amount of metal back donation is certainly operative. At lower energy, other filled levels have lone-pair character at the other P atoms of the P_4 unit but, just because of this, they are evidently less favoured for the electrophilic attack.

Conclusion

The reaction of the rhodium synthon [(triphos)RhR] (R = H, Me, Et, Ph) and white phosphorus results in the formation of a new family of complexes of formula [(triphos)Rh($\eta^1{:}\eta^2$-P_4R)] that feature the unprecedented P_4R ligand moiety with a total of four electrons, a $\eta^1{:}\eta^2$ ligand. While reflux conditions are necessary to generate the [(triphos)RhH] moiety from [(triphos)RhH_3] by H_2 elimination, the [(triphos)RhR] fragment may be produced under very mild conditions by the facile elimination of ethylene from the complex [(triphos)Rh$R(C_2H_4)$]. In the case of the hydridoethene derivatives, a double-insertion reaction occurs that leads to [(triphos)Rh($\eta^1{:}\eta^2$-P_4Et)].

Compounds [(triphos)Rh($\eta^1{:}\eta^2$-P_4R)] are thermally unstable with respect to the formation of [(triphos)Rh(η^3-P_3)] (**3**) and a variety of unknown phosphorus species (^{31}P NMR analysis). In the case of the hydridotetraphosphido derivative, the formation of **3** is accompanied by the evolution of PH_3 in almost quantitative yield. In high-pressure experiments phosphine and PH_2R are produced, the latter in less than 15% yield, when the decomposition is carried out under hydrogen.[10g, 53]

Electrophilic attack by H^+ and carbocations is a straightforward reaction that results in the formation of the cationic derivatives [(triphos)Rh($\eta^1{:}\eta^2$-P_4RR')]Y by selective attack to the monosubstituted phosphorus atom of the $\eta^1{:}\eta^2$-P_4R substituent. The total regioselectivity of the attack is fully confirmed by DFT calculations on a series of alternative isomers and their different energetics. The theoretical analysis also allows a reasonable description of the chemical bonding in these compounds.

A detailed NMR investigation of both neutral $\eta^1{:}\eta^2$-P_4R and cationic $\eta^1{:}\eta^2$-P_4RR' complexes has allowed us to define in detail their solution structure, which matches that determined for **12** in the solid state by X-ray methods.

As a final conclusion, it should be stressed that the tetraphosphorus derivatives presented in this paper are intriguing compounds because they represent, to the best of our knowledge, the first documented example of white phosphorus functionalisation mediated by a transition metal system in which an alkyl or aryl group is smoothly and directly transferred from a transition metal centre to one of the four phosphorus atoms of the P_4 phosphorus allotrope.

Moreover, the protocol of functionalising white phosphorus described in this paper is exciting because it represents a useful model for the development of a catalytic tool to circumvent the use of chlorine in manufacturing organophosphorus compounds from white phosphorus. Studies are in progress to explore the applications of these reactions and to seek a rhodium complex capable of providing a catalytic access to organophosphorus compounds from P_4 and alcohols.

Acknowledgements

This work was supported by INTAS (Brussels, Belgium) through project 00–00018 ("Towards an Ecoefficient Functionalisation of White Phosphorus") and by the Deutschen Forschungsgemeinschaft through the program Graduiertenkolleg ("Phosphorus as a Link between Different Chemical Disciplines") with a mobility grant to supporting the *stage* of G.S. in Florence. M.P. wish to express his gratitude to Dr. Markus Ehses, University of Saarbrucken, Germany, for reading the manuscript and for helpful suggestions. A.I. and C.M. are grateful for the computing time provided by CINECA, under the agreement with the CNR.

[1] a) Ya. A. Dorfman, M. M. Aleshkova, G. S. Polimbetova, L. V. Levina, T. V. Petrova, R. R. Abdreimova, D. M. Doroshkevich, *Russ. Chem. Rev.* **1993**, *62*, 877; b) J. I. Heise, E. D. Sall, M. P. McGrath, *International Patent* WO 99/43612; c) C. Bianchini, M. Peruzzini, D. Akbayeva, R. R. Abdreimova, G. S. Polimbetova, *Italian Patent* 2202/2PTIT; d) M. Peruzzini, *Spec. Chem. Mag.* **2003**, 32.

[2] D. E. C. Corbridge, *Phosphorus – an Outline of its Chemistry, Biochemistry and Technology*, 5th ed., Elsevier, Amsterdam (Netherlands), **1995**.

[3] a) I. Krossing, *J. Am. Chem. Soc.* **2001**, *123*, 4603; b) I. Krossing, L. van Wüllen, *Chem. Eur. J.* **2002**, *8*, 700. For a theoretical analysis of the bonding in the $(\eta^2\text{-}P_4)]^+$ cation, see: D. V. Deubel, *J. Am. Chem. Soc.* **2002**, *124*, 12312.

[4] A. P. Ginsberg, W. E. Lindsell, *J. Am. Chem. Soc.* **1971**, *93*, 2082. For a complete characterisation of this compound, see: A. P. Ginsberg, W. E. Lindsell, K. J. McCullough, C. R. Sprinkle, A. J. Welch, *J. Am. Chem. Soc.* **1986**, *108*, 403.

[5] Other η^2-P_4 complexes: a) $[Cp''M(\eta^2\text{-}P_4)]$ (M = Zr, Hf): O. J. Scherer, M. Swarowsky, G. Wolmershäuser, *Angew. Chem.* **1988**, *100*, 738; *Angew. Chem. Int. Ed. Engl.* **1988**, *27*, 694. $[Cp^*Co(CO)(\eta^2\text{-}P_4)]$: O. J. Scherer, M. Swarowsky, G. Swarowsky, G. Wolmershäuser, *Organometallics* **1989**, *8*, 841; b) $[\{Cp''Co(CO)\}(\eta^{2:1:1:1:1}\text{-}P_4)\{Cr(CO)_5\}_4]$: M. Scheer, U. Becker, C. J. Huffman, M. H. Chisholm, *J. Organomet. Chem.* **1993**, *461*, C1; c) M. Scheer, U. Becker, *J. Organomet. Chem.* **1997**, *545/546*, 451; d) $[\{CpRh(CO)\}(\eta^{2:1:1:1:1}\text{-}P_4)\{Cr(CO)_5\}_4]$: M. Scheer, C. Troitzsch, L. Hilfert, M. Dargatz, E. Kleinpeter, P. G. Jones, J. Sieler, *Chem. Ber.* **1995**, *128*, 251; e) $[\{Cp^*Ir(CO)\}(\eta^{2:1:1:1:1}\text{-}P_4)\{Cr(CO)_5\}_4]$: M. Scheer, U. Becker, E. Matern, *Chem. Ber.* **1996**, *129*, 721; f) $[(PPh_3)_2Pt(\eta^{2:1:1}\text{-}P_4)\{Cr(CO)_5\}_2]$: M. Scheer, M. Dargatz, A. J. Rufinska, *Organomet. Chem.* **1992**, *440*, 327.

[6] O. J. Scherer, T. Hilt, G. Wolmershäuser, *Organometallics* **1998**, *17*, 4110.

[7] M. Ehses, A. Romerosa, M. Peruzzini, *Top. Curr. Chem.* **2002**, *220*, 108.

[8] M. Peruzzini, I. de los Ríos, A. Romerosa F. Vizza, *Eur. J. Inorg. Chem.* **2001**, 593.

[9] P. J. Chirik, J. A. Pool, E. Lobkowsky, *Angew. Chem.* **2002**, *114*, 3613; *Angew. Chem. Int. Ed.* **2002**, *41*, 3463.

[10] a) I. de los Ríos, J.-R. Hamon, P. Hamon, C. Lapinte, L. Toupet, A. Romerosa, M. Peruzzini, *Angew. Chem.* **2001**, *113*, 4028; *Angew. Chem. Int. Ed*. **2001**, *40*, 3910; b) M. Di Vaira, M. P. Ehses, M. Peruzzini, P. Stoppioni, *Eur. J. Inorg. Chem.* **2000**, 2193; c) M. Peruzzini, S. Mañas, A. Romerosa, A. Vacca, *Mendeleev Commun.* **2000**, 134; d) M. Di Vaira, M. P. Ehses, M. Peruzzini, P. Stoppioni, *Inorg. Chem.* **2000**, *39*, 2199; e) M. Di Vaira, M. P. Ehses, M. Peruzzini, P. Stoppioni, *J. Organomet. Chem.* **2000**, *593/594*, 127; f) M. Peruzzini, L. Marvelli, A. Romerosa, R. Rossi, F. Vizza, F. Zanobini, *Eur. J. Inorg. Chem.* **1999**, 931; g) M. Peruzzini, J. A. Ramirez, F. Vizza, *Angew. Chem.* **1998**, *110*, 2376; *Angew. Chem. Int. Ed*. **1998**, *37*, 2255.

[11] a) O. J. Scherer, *Acc. Chem. Res.* **1999**, *32*, 751; b) O. J. Scherer, *Chem. Unserer Zeit* **2000**, *34*, 374; c) O. J. Scherer, *Angew .Chem.* **1990**, *102*, 1137; *Angew. Chem. Int. Ed. Engl.* **1990**, *29*, 1104.

[12] P. Barbaro, M. Peruzzini, J. A. Ramirez, F. Vizza, *Organometallics* **1999**, *18*, 4237.

[13] J. I. Heise, M. Yinong, *European Patent* EP 1008552 A1; H.-J. Sterzel, A. Brand, *International Patent* WO 01/51416 A1.

[14] J. Ott, L. M. Venanzi, C. A. Ghilardi, S. Midollini, A. Orlandini, *J. Organomet. Chem.* **1985**, *291*, 89.

[15] C. Bianchini, A. Meli, M. Peruzzini, F. Vizza, P. Frediani, J. A. Ramirez, O*rganometallics* **1990**, *9*, 226.

[16] V. Bakhmutov, C. Bianchini, M. Peruzzini, F. Vizza, E. Vorontsov, *Inorg. Chem.* **2000**, *39*, 1655, and references therein.

[17] P. H. M. Budzelaar, *gNMR* V4.0, Cherwell Scientific Publishing, Copyright **1995–1997** Ivory soft.

[18] A. Derome, M. Williamson, *J. Magn. Reson.* **1990**, *88*, 177.

[19] V. Sklener, H. Miyashiro, G. Zon, H. T. Miles, A. Bax, *FEBS Lett.* **1986**, *208*, 94; b) J. Jeener, B. H. Meier, P. Bachmann, R. R. Ernst, *J. Chem. Phys.* **1979**, *71*, 4546.

[20] A. Bax, R. H. Griffey, B. L. Hawkins, *J. Magn. Reson.* **1983**, *55*, 301.

[21] a) A. Bax, M. F. Summers, *J. Am. Chem. Soc.* **1986**, *108*, 2093; b) M. F. Summers, L. G. Marzilli, A. Bax, *J. Am. Chem. Soc.* **1986**, *108*, 4285.

[22] a) H. Rüegger, P. S. Pregosin, *Inorg. Chem.* **1987**, *26*, 2912; b) C. Amman, P. S. Pregosin, A. Scrivanti, *Inorg. Chim. Acta.* **1989**, *155*, 217.

[23] C. Bianchini, A. Meli, A. Traversi, *Italian Patent* FI A000025, **1997**.

[24] C. Bianchini, C. Mealli, A. Meli, L. Sacconi, *Inorg. Chim. Acta* **1979**, *37*, L54.

[25] SHELX, G. M. Sheldrick, University of Göttingen, Germany, **1997**.

[26] SHELXTL, Bruker AXS, Karlsruhe, Germany, **1998**.

[27] A. D. Becke, *J. Chem. Phys.* **1993**, *98*, 5648.

[28] C. Lee, W. Yang, R. Parr, *G. Phys. Rev.* **1998**, *B37*, 785.

[29] Gaussian 98 (Revision A.9), M. J. Frisch, G. W. Trucks, H. B. Schlegel, G. E. M. Scuseria, A. Robb, J. R. Cheeseman, V. G. Zakrzewski, J. A. Montgomery, R. E. Stratmann, J. C. Burant, S. Dapprich, J. M. Millam, A. D. Daniels, K. N. Kudin, M. C. Strain, O. Farkas, J. Tomasi, V. Barone, M. Cossi, R. Cammi, B. Mennucci, C. Pomelli, C. Adamo, S. Clifford, J. Ochterski, G. A. Petersson, P. Y. Ayala, Q. Cui, K. Morokuma, D. K. Malick, A. D. Rabuck, K. Raghavachari, J. B. Foresman, J. Cioslowski, J. V. Ortiz, B. B. Stefanov, G. Liu, A. Liashenko, P. Piskorz, I. Komaromi, R. Gomperts, R. L. Martin, D. J. Fox, T. Keith, M. A. Al-Laham, C. Y. Peng, A. Nanayakkara, C. Gonzalez, M. Challacombe, P. M. W. Gill, B. G. Johnson, W. Chen, M. W. Wong, J. L. Andres, M. Head-Gordon, E. S. Replogle, J. A. Pople, Gaussian Inc., Pittsburgh, PA, **1998**.

[30] P. J. Hay, W. R. Wadt, *J. Chem. Phys.* **1985**, *82*, 299.

[31] P. C. Hariharan, J. A. Pople, *Theor. Chim. Acta* **1973**, *28*, 213.

[32] C. Mealli, D. M. Proserpio, *J. Chem. Educ.* **1990**, *67*, 399; C. Mealli, A. Ienco, D. M. Proserpio, *Book of Abstracts of the XXXIII ICCC*, Florence, Italy, **1998**, 510.

[33] a) R. Hoffmann, W. N. Lipscomb, *J. Chem. Phys.* **1962**, *36*, 2872; b) R. Hoffmann, W. N. Lipscomb, *J. Chem. Phys.* **1962**, *37*, 3489.

[34] a) S. Midollini, A. Orlandini, L. Sacconi, *Angew. Chem.* **1979**, *91*, 93; *Angew. Chem. Int. Ed. Engl.* **1979**, *18*, 81; b) M. Di Vaira, P. Stoppioni, M. Peruzzini, *J. Chem. Soc. Dalton Trans.* **1990**, 109; c)) M. Di Vaira, D. Rovai, P. Stoppioni, *Polyhedron* **1990**, *9*, 2477; d) M. Di Vaira, M. P. Ehses, P. Stoppioni, M. Peruzzini, *Polyhedron* **1999**, *18*, 2331.

[35] a) G. Capozzi, L. Chiti, M. Di Vaira, M. Peruzzini, P. Stoppioni, *J. Chem. Soc. Chem. Commun.* **1986**, 1799; b) A. Barth, G. Huttner, M. Fritz, L. Zsolnai, *Angew. Chem.* **1990**, *102*, 956; *Angew. Chem. Int. Ed. Engl.* **1990**, *29*, 929.

[36] *Chemical Society Special Publication No. 18*, Chemical Society, London, **1968**.

[37] C. Mealli, F. Costanzo, A. Ienco, M. Peruzzini, E. Perez-Carreño, *Inorg. Chim. Acta.* **1998**, *275–276*, 366.

[38] A. H. Cowley, J. E. Kilduff, J. G. Lasch, S. K. Mehrotra, N. C. Norman, M. Pakulski, B. R. Whittlesey, J. L. Atwood, W. E. Hunter *Inorg.-Chem.* **1984**, *23*, 2582.

[39] I. G. Phillips, R. G. Ball, R. G. Cavell *Inorg. Chem.* **1992**, *31*, 1663, **1992**.

[40] M. Murray in *Phosphorus-31 NMR Spectral Properties in Compound Characterization and Structural Analysis*, (Eds.: J. G. Verkade, L. D. Quin), Wiley, New York, **1994**, p, 347.

[41] A. L. Crumbliss, R. J. Topping in *Methods in Stereochemical Analysis 8: Phosphorus-31 NMR Spectroscopy in Stereochemical Analysis*, (Eds.: J. G. Verkade, L. D. Quin) VCH, Weinheim, Germany, **1987**, p. 531.

[42] P. S. Pregosin, R. W. Kunz, *^{31}P and ^{13}C NMR of Transition Metal Phosphine Complexes* (Eds.: P. Diehl, E. Fluck, R. Kosfeld), Springer, Berlin, Germany, **1979**.

[43] a) H. Schäfer, D. Binder, *Z. Anorg. Allg. Chem.* **1988**, *557*, 45; b) A. H. Cowley, N. C. Norman, *Prog. Inorg. Chem.* **1986**, *34*, 1.

[44] P. Lorenzo, I. de los Ríos, M. Peruzzini, *Phosphorus Res. Bull.* **2001**, *12*, 167.

[45] D. W. Meek, T. J. Mazanec, *Acc. Chem. Res.* **1981**, *14*, 266.

[46] T. G. Appleton, H. C. Clark, L. E. Manzer, *Coord. Chem. Rev.* **1973**, *10*, 335.

[47] J. G. Verkade, J. A. Mosbo in *Methods in Stereochemical Analysis 8: Phosphorus-31 NMR Spectroscopy in Stereochemical Analysis* (Eds.: J. G. Verkade, L. D. Quin), VCH, Weinheim, Germany, **1987**, p. 432.

[48] Only for $[(triphos)Rh(\eta^1\text{:}\eta^2\text{-}P_4H)]$ (**2**) was the $^1H-^{31}P$ correlation optimised for the large $^1J_{HP}$ scalar coupling ($^1J_{HP} = 120$ Hz).

[49] A study of the ^1H NOESY spectra of the $[(triphos)Rh(\eta^1\text{:}\eta^2\text{-}P_4RR')]^+$ complexes indicates the occurrence of fluxional behaviour in these compounds. Analysis and mechanistic investigation of the dynamic of the process is currently being pursued in our laboratory and will be published in due course.

[50] W. E. Hull in *Two-Dimensional NMR Spectroscopy Applications for Chemists and Biochemists* (Eds.: W. R. Croasmun, R. M. K. Carlson), VCH, Weinheim, Germany, **1994**, pp. 327 – 333.
[51] The NOEs to the *ortho* protons pointed out that, in the cationic complexes **11** and **12**, the R′ substituents (R′ = H, Me) face the $Ph'P_B$ phenyl.
[52] A. E. Reed, L. A. Curtis, F. Weinhold, *Chem. Rev.* **1988**, *88*, 899.
[53] The reactivity of the $[(triphos)Rh(\eta^1{:}\eta^2\text{-}P_4RR')]^{n+}$ complexes described in this article is currently under study and will be presented in due time together with an in-depth mechanistic investigation of the whole metal-mediated P_4 activation process.

Received: April 30, 2003 [F5091]